thereby allowing hydration-free CDDP treatment for the improvement of the patients' QOL.

CDDP-induced hearing loss is usually bilateral, irreversible, and cumulative. Audiological studies have indicated that up to 90% of the patients receiving CDDP experience significant hearing loss, especially at high frequencies [9]. The CDDP-induced hearing loss is particularly serious in pediatric populations because loss of hearing at this developmental stage hampers speech and cognitive and social development. Therefore, there is an imperative need for developing treatments that will ameliorate CDDP-induced ototoxicity. However, to date, no such cures or preventive treatments are available. In the present study, we evaluated the ototoxicity of polymeric micelles incorporating CDDP (NC-6004) in comparison with that of CDDP. NC-6004 has been evaluated in a phase I clinical trial in the United Kingdom [10], and the phase I/II trial is now underway in East Asia.

2. Materials and Methods

2.1. Materials

CDDP was purchased from WC Heraeus GmbH & Co., KG (Hanau, Germany). NC-6004 was prepared according to the slightly modified procedure that was previously reported [11] and supplied by NanoCarrier Co. Ltd. (Chiba, Japan). In brief, NC-6004 is a polymer–metal complex micelle comprising CDDP and sodium salt of poly (ethylene glycol)–poly(glutamic acid) block copolymer [PEG-P(Glu)] [11].

2.2. Animals

We used 20 healthy male Hartley-strain albino guinea pigs (weighing 243–314 g; Saitama Experimental Animals Supply Co. Ltd., Japan) with normal Preyer's reflex. The animals were housed, 5 together, in animal cages and given free access to food and water. A 12-hour dark-light cycle was maintained. They were anesthetized with a mixture of ketamine hydrochloride (40 mg/kg; Daiichi Sankyo Prophama Co. Ltd., Japan) and xylazine hydrochloride (10 mg/kg; Bayer Healthcare, Germany) during all measurements and intravenous injection procedures. All animal experiments conformed to the guidelines of the University Committee for the Use and Care of Animals, University of Tokyo, and the National Institutes of Health Guide for the Care and Use of Laboratory Animals.

2.3. Drug administration

The animals were divided into five groups according to the drug administered. Groups Cis(8) ($n=4$) and Cis(12) ($n=6$) received a bolus intravenous injection of 8 and 12 mg/kg CDDP, respectively, as well as 20 ml normal saline subcutaneously immediately after the injection to decrease the renal damage. Groups Cis-m(8) ($n=3$) and Cis-m(12) ($n=4$) received a bolus intravenous injection of NC-6004 comprising 8 and 12 mg/kg CDDP, respectively, but no subcutaneous hydration. The control group ($n=3$) received normal saline intravenously.

2.4. Auditory brainstem response measurement

Auditory brainstem responses (ABRs) were measured before and 5 days after the drug administration. The tympanic membranes were examined before the recording to ensure normal middle ear appearance. Needle electrodes were placed subcutaneously at the vertex (active electrode), beneath the pinna of the left ear (reference electrode), and beneath the right ear (ground electrode). The sound stimulus consisted of a 7 ms tone burst with a rise-fall time of 1 ms at 2, 6, 12, 20, and 30 kHz. The ABRs to 500 sweeps were averaged at each intensity level (5 dB steps) to assess the threshold, which was defined as the lowest intensity level at which a clear reproducible waveform is visible in the trace. When an ABR waveform could not be evoked, the threshold was assumed to be 5 dB greater than the maximum intensity produced by the system (105 dB sound pressure level). Threshold shifts were calculated by subtracting the pre-administration thresholds from the post-administration thresholds.

2.5. Hair-cell count

The animals in groups Cis(12) and Cis-m(12) were sacrificed under deep anesthesia after the ABR measurements and their left temporal bone was removed. The cochleae were harvested from the temporal bone and perfused with 4% paraformaldehyde in 0.1 M phosphate buffer (PFA) through a perforation in the apex and the opened oval window. They were postfixed in 4% PFA overnight and stored at 4 °C. PFA was removed by rinsing the samples in phosphate-buffered saline (PBS). The lateral wall, tectorial membrane, and Reissner's membrane were removed, and the cochlear sensory epithelium was detached from the bony shell. The epithelial cells were permeabilized in 0.3% Triton X-100 in PBS for 10 min, rinsed in PBS, stained with 1% rhodamine-phalloidin (Sigma Chemical Co., St. Louis, MO, USA) for 40 min, and once again rinsed in PBS. The organ of Corti was separated from the modiolus and mounted on glass slides. Surface preparation assessment was performed under confocal microscopy (LSM 510 META, Carl Zeiss, Inc., Jena, Germany). The total numbers of hair cells and damaged hair cells were counted from the apex to the basal turn. For the analysis of each cochlea, the whole length of the basilar membrane except the hook was assessed. A cytocochleogram was prepared by plotting the mean percentage of missing hair cells as a function of the percentage length of the organ of Corti.

2.6. Platinum distribution and concentration measurement

Synchrotron radiation-induced X-ray fluorescence spectrometry (μSR-XRF) imaging was performed to determine the platinum distribution in sections of the organ of Corti from groups Cis(12) and Cis-m(12). The left temporal bone was removed, surface preparation of the organ of Corti was performed as mentioned in the preceding, and the samples were fixed on polypropylene sheets. μSR-XRF was performed by using beam line 37XU at SPring-8 (Hyogo, Japan), at 8 GeV and about 100 mA. A photon beam with energy of 14 keV, a beam-spot size of $1.3\times1.3\ \mu m^2$, and intensity of 10^{12} photons/s was irradiated on the tissue samples. The fluorescence X-rays were measured by using a Si-SSD (Silicon solid state detector) in air at room temperature. The samples on the acryl board were then mounted on an x–y translation stage. The fluorescence X-ray intensity was normalized to the incident X-ray intensity, I_0, to produce a two-dimensional elemental map. Tissue sections of $250\times250\ \mu m^2$ were roughly scanned before the imaging. The count of platinum atoms in the samples was converted to the concentration of platinum by using the calibration standards (10 and 500 μM) of CDDP. The total intensity per tissue area was determined by using ImageJ 1.43u software (US National Institutes of Health).

2.7. Statistical analysis

We used SigmaStat software (Systat Software, Inc., Chicago, IL, USA) for statistical analysis. The ABR threshold shifts at each frequency were compared among the control and experimental groups. Bartlett's test was used to test the normality of the distribution, and one-way analysis of variance (ANOVA), Tukey–Kramer or Kruskal–Wallis test, or Dunn's test was used according to the distribution. The survival rates of the inner and outer hair cells in groups Cis(12) and Cis-m(12) were compared by using a two-tailed Student's t-test. A value of $P<0.05$ was considered statistically

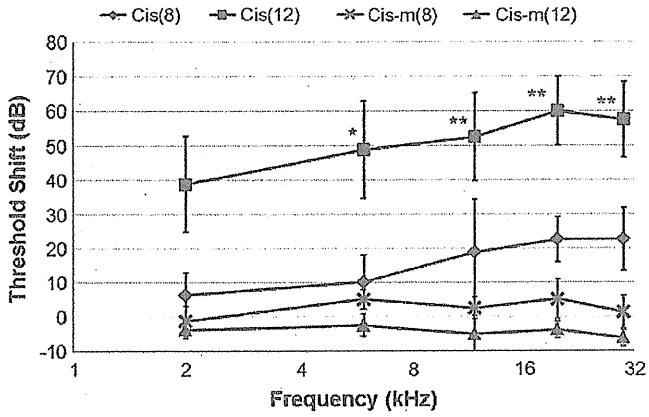

Fig. 1. ABR threshold shifts from the baseline to five days after drug administration. All results represent the mean ± SEM. *$P \leq 0.05$, **$P < 0.01$.

significant. The data were calculated as the mean ± standard error of the mean (SEM).

3. Results

Two animals in group Cis(12) died within four days of the 12 mg/kg CDDP administration (33% mortality), and were thus excluded from the data analysis. The LD_{50} for a single injection of CDDP is 9.7 mg/kg in guinea pigs [12].

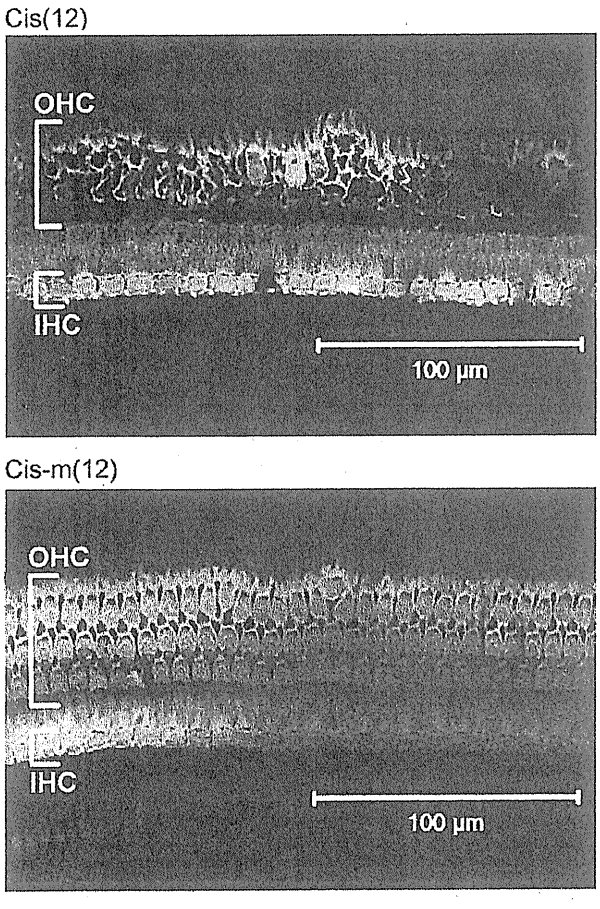

Fig. 2. Representative rhodamine-phalloidin-stained sections of the organ of Corti in the basal turn in groups Cis(12) (left) and Cis-m(12) (right). Three rows of the outer hair cells (OHCs) and a single row of the inner hair cells (IHCs) are well preserved in an animal treated with Cis-m(12), whereas almost all of the OHCs and a few IHCs are missing in an animal treated with Cis(12).

3.1. ABR threshold shifts

The ABR threshold shifts of the experimental groups are shown in Fig. 1. Group Cis(8) showed mild ABR threshold shifts (range = 6–23 dB) at the measured frequencies, but group Cis(12) demonstrated larger shifts (range = 39–60 dB) that were more severely affected by the higher frequencies. In contrast, groups Cis-m(8) and Cis-m(12) showed virtually no ABR threshold shifts. The Cis(8) ABR thresholds tended to be more affected than the Cis-m(8) ABR thresholds, although the differences between the groups were not statistically significant. Groups Cis(12) and Cis-m(12) had significant differences at all frequencies ($P < 0.05$ at 2 kHz and $P < 0.01$ at 6, 12, 20, and 30 kHz).

3.2. Hair-cell survival rates

In the normal organ of Corti, 3 rows of the outer hair cells (OHCs) and a single row of the inner hair cells (IHCs) can be observed. Fig. 2 shows the representative rhodamine-phalloidin-stained organ of Corti in the basal turn in groups Cis(12) and Cis-m(12). Significant damage of the OHCs and mild damage of the IHCs were observed in group Cis(12), whereas only few notable damages were observed in both the IHCs and OHCs in group Cis-m(12).

In terms of the IHC survival rates (Fig. 3A), approximately 10% of the IHCs were lost in group Cis(12) group, whereas less than 3% of these hair cells were lost in group Cis-m(12). Between the groups, significant differences in the IHC survival rate were noted at the distances of 30%, 40%, 70%, and 80% from the apex ($P < 0.05$). The difference was also significant when the total IHC loss was compared ($P < 0.05$).

Fig. 3B shows the survival rates of the OHCs in groups Cis(12) and Cis-m(12). Approximately 50% of these hair cells were lost in group Cis(12), whereas less than 15% were lost in group Cis-m(12). In group Cis(12), the extent of OHC loss ranged from 21% at 10% from the apex to 68% at 80% from the apex, indicating that the basal region was more severely affected than the apical region. Comparatively, the animals in group Cis-m(12) showed less damage in the OHCs, but similarly, the basal region was more severely affected than the apical region: the extent of OHC loss was less than 20% in all the segments except 90% from the apex (25% loss). These groups showed significant differences in the OHC survival rates at the distances of 20%, 40%, and 60–90% from the apex ($P < 0.05$). The difference was also significant when the total OHC loss was compared ($P < 0.05$).

3.3. Platinum distribution and concentration

Fig. 4 shows the platinum distribution in the organ of Corti in groups Cis(12) and Cis-m(12). Group Cis(12) had an apparently higher platinum concentration in the organ of Corti than group Cis-m(12). The mean intensity of platinum per tissue area of the organ of Corti (count/mm^2) was significantly greater in group Cis(12) than in group Cis-m(12) ($P < 0.01$; Table 1).

4. Discussion

The main targets of CDDP in the cochlea are the OHCs in the organ of Corti and the stria vascularis, the vascularized epithelium in the cochlear lateral wall [13]. CDDP induces a caspase-dependent apoptotic pathway in these sensitive cochlear cells [14]. The molecular mechanisms that trigger apoptosis in the cochlea have not been elucidated, but several mechanisms have been proposed, such as increased generation of reactive oxygen species [13,15]. Platinum analogs, such as carboplatin [16] and oxaliplatin [17], have been developed to overcome the CDDP-related side effects. However, clinical trials have shown that the regimens including CDDP are still the most useful platinum-containing antineoplastic drugs [18]. Dozens of experimental studies have attempted to find ideal protective agents

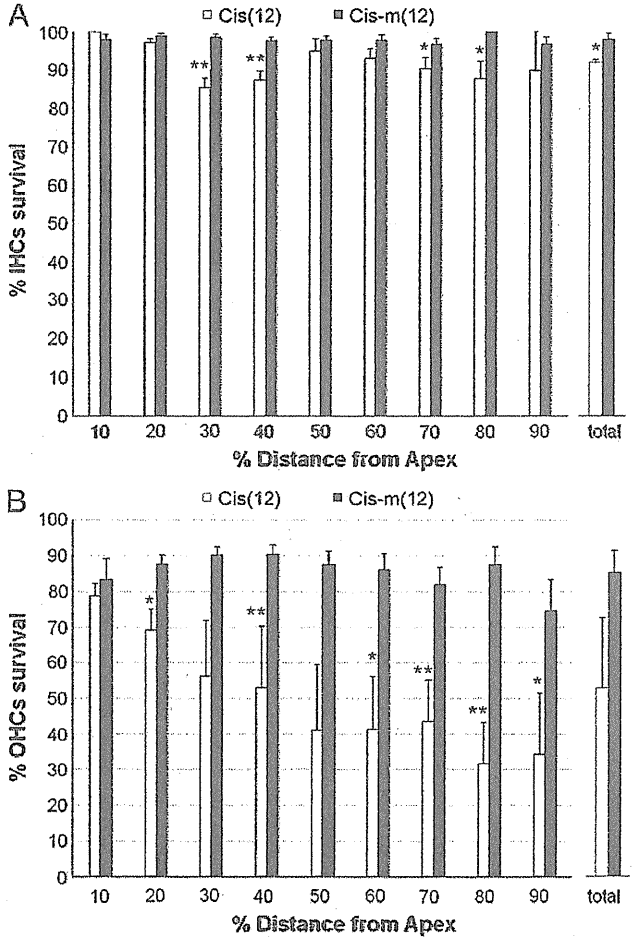

Fig. 3. Survival rates of the inner and outer hair cells in groups Cis(12) and Cis-m(12) determined five days after drug administration by using cytocochleograms. The survival rates of the inner (A) and outer (B) hair cells were calculated as percentages of the number of surviving hair cells in the experimental groups to that in the control group in each field. The results represent the mean ± SEM (n = 4 guinea pigs in each group). *P < 0.05, **P < 0.01.

against CDDP ototoxicity. Previous studies have shown that antioxidants, including sodium thiosulfate [19], D- or L-methionine [20,21], diethyldithiocarbamate [22,23], lipoic acid [24], and N-acetylcysteine [25], are useful in scavenging reactive oxygen species in the inner ear. However, systemic administration of L-methionine or sodium thiosulfate may inactive CDDP and reduces its antitumor activity. To prevent CDDP ototoxicity without reducing its antitumor activity, these agents require invasive approaches for delivery into the inner ear. Several other agents that protect from CDDP ototoxicity and also preserve its antitumor effect have been developed; round window application of adenosine A1 receptor agonists [26,27] and oral administration of ebselen and allopurinol [28], sodium butyrate [29], and salicylates [30] are partially effective in reducing CDDP ototoxicity without affecting its antitumor activity in animals. Until now, however, no clinical interventions have been shown to prevent CDDP ototoxicity and ensure safe therapy without reduced antitumor activity [31]. The development of a drug-delivery technology offering better selective accumulation of CDDP in solid tumors while lessening its distribution in normal tissues is therefore anticipated.

In this study, we evaluated the ototoxicity of NC-6004 and CDDP, and found that the animals given NC-6004 intravenously showed virtually no ABR threshold shifts, excellent inner and outer hair-cell preservation, and reduced platinum distribution and concentration in the organ of Corti compared with those that received the same doses of cisplatin. These results clearly indicate the markedly less-extensive ototoxicity of NC-6004.

The organ of Corti is isolated from the systemic circulation by the blood–cochlear barrier, which is similar to the blood–brain barrier [32]. CDDP readily penetrates this barrier and enters the perilymph of the inner ear, where it reaches the hair cells and exerts its toxic action. The limited cochlear uptake of oxaliplatin is considered responsible for the lower ototoxicity of oxaliplatin than CDDP [33]. The particle size of NC-6004 is approximately 30 nm [11] and that of the intrastrial space is approximately 15 nm [33,34]; therefore, the decreased ototoxicity of NC-6004 is mainly attributable to its circumvention of the IHCs and OHCs by not crossing the stria vascularis, which forms a part of the blood–cochlear barrier.

In the current study, the differences in the platinum distribution between animals treated with CDDP and NC-6004 were elucidated by

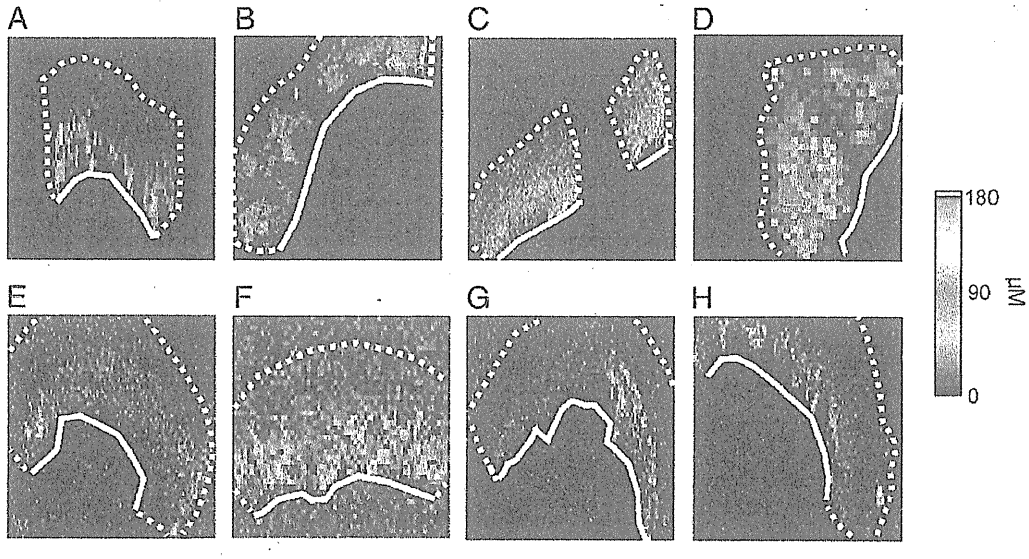

Fig. 4. Synchrotron radiation-induced X-ray fluorescence spectrometry images of the platinum distribution and concentration in the organ of Corti. The white lines indicate the basilar membrane and the areas surrounded by the broken lines indicate the presence of platinum. The cochlear epithelium in groups (A–D) Cis(12) and (E–H) Cis-m(12) at distances of approximately 20%, 40%, 60%, and 80% from the apex are shown.

Table 1
The mean intensity of platinum per tissue area (count/mm^2) shown in Fig. 4.

Group	Figure	Tissue area intensity	Background intensity	Tissue area-to-background intensity ratio
Cis(12)	A	22.06	3.39	6.51
Cis(12)	B	6.55	0.95	6.93
Cis(12)	C	21.99	3.85	5.72
Cis(12)	D	67.68	10.07	6.72
Average				6.47
Cis-m(12)	E	6.92	4.29	1.61
Cis-m(12)	F	48.81	33.63	1.45
Cis-m(12)	G	10.27	5.79	1.77
Cis-m(12)	H	8.92	5.39	1.65
Average				1.62

The data were rounded off to the second decimal place.

μSR-XRF. Until now, 2 sampling techniques have been used to measure the platinum concentration in the cochlea: sampling of the perilymph in the scala tympani [33] and homogenizing the cochlear tissue [35]. In either of the techniques, it is impossible to measure the platinum concentration only in the organ of Corti. In contrast, μSR-XRF enables (semi-)quantitative measurement of platinum concentration in the organ of Corti. The limitation of our technique is that its resolution is not high enough to distinguish each cell in the organ of Corti, which contains not only the hair cells but also the supporting cells. Thus, we could not measure the platinum concentration exclusively in the hair cells, one of the main targets of CDDP-induced cell damage. However, a previous immunohistochemical study [36], in which the CDDP was detected indirectly in the guinea pig cochlea by using an antiserum containing antibodies against CDDP-DNA adducts, showed that, while platinated DNA was present in the nuclei of most cells in the organ of Corti after CDDP administration, the nuclei of the OHCs exhibited prominent immunostaining, with the nuclei of all other (supporting) cells being only weakly stained. Therefore, it is reasonable that the platinum concentration in the organ of Corti measured by μSR-XRF is mainly derived from the OHCs.

Reportedly, there is a large difference in the CDDP concentration between the perilymph and the blood, and ABR threshold shifts are related to the CDDP concentration in the blood but not in the perilymph [37]. These findings suggest that a high plasma concentration of CDDP could collapse the blood–cochlear barrier at the initial stage after CDDP administration. NC-6004 is a long-circulating carrier with a gradual-release profile of CDDP [11]. Therefore, the reduced ototoxicity of NC-6004 can also be explained by the possibility that the gradual-release profile of CDDP from NC-6004 avoids an abrupt transient increase in the plasma CDDP concentration at the initial stage after its administration, thereby preserving the blood–cochlear barrier. This view is consistent with the fact that NC-6004 has negligible nephrotoxicity compared with CDDP, which shows a transient increase in its initial blood concentration [7]. There is also a significant correlation between the plasma creatinine level, an indicator of renal function, and the concentration of platinum [38]. Therefore, the reduced nephrotoxicity of NC-6004 might contribute to its reduced ototoxicity.

5. Conclusion

The present study demonstrated that the systemic administration of CDDP induced dose-dependent ABR threshold shifts and hair cell damage in guinea pigs, whereas such adverse effects were virtually absent after the systemic administration of NC-6004. The μSR-XRF imaging showed that the platinum distribution in the organ of Corti was significantly reduced by the micellization of CDDP. These findings confirm that the micellization of CDDP reduces its ototoxicity without additional administration of protective agents, and these findings have not been reported in previous studies. This advantage will improve patient compliance in cancer chemotherapy while maintaining substantial antitumor efficacy.

Acknowledgements

This research was supported by the Funding Program for World-Leading Innovative R&D on Science and Technology (FIRST Program) of the Japan Society for the Promotion of Science (JSPS) (to K.K.), the Core Research Program for Evolutional Science and Technology (CREST) of the Japan Science and Technology Corporation (JST) (to K.K.), and Grants-in-Aid for Scientific Research from the Japanese Ministry of Education, Culture, Sports, Science and Technology (to Y.M. and T.Y.).

References

[1] P.A. Vasey, S.B. Kaye, R. Morrison, C. Twelves, P. Wilson, R. Duncan, A.H. Thomson, L.S. Murray, T.E. Hilditch, T. Murray, S. Burtles, D. Fraier, E. Frigerio, J. Cassidy, Phase I clinical and pharmacokinetic study of PK1 [N-(2-hydroxypropyl) methacrylamide copolymer doxorubicin]: first member of a new class of chemotherapeutic agents-drug-polymer conjugates. Cancer Research Campaign Phase I/II Committee, Clin. Cancer Res. 5 (1999) 83–94.
[2] T. Lian, R.J. Ho, Trends and developments in liposome drug delivery systems, J. Pharm. Sci. 90 (2001) 667–680.
[3] M.E. Davis, Z.G. Chen, D.M. Shin, Nanoparticle therapeutics: an emerging treatment modality for cancer, Nat. Rev. Drug Discov. 7 (2008) 771–782.
[4] M. Orditura, F. Quaglia, F. Morgillo, E. Martinelli, E. Lieto, G. De Rosa, D. Comunale, M.R. Diadema, F. Ciardiello, G. Catalano, F. De Vita, Pegylated liposomal doxorubicin: pharmacologic and clinical evidence of potent antitumor activity with reduced anthracycline-induced cardiotoxicity (review), Oncol. Rep. 12 (2004) 549–556.
[5] Y. Matsumura, H. Maeda, A new concept for macromolecular therapeutics in cancer chemotherapy: mechanism of tumoritropic accumulation of proteins and the antitumor agent smancs, Cancer Res. 46 (1986) 6387–6392.
[6] T. Hamaguchi, Y. Matsumura, M. Suzuki, K. Shimizu, R. Goda, I. Nakamura, I. Nakatomi, M. Yokoyama, K. Kataoka, T. Kakizoe, NK105, a paclitaxel-incorporating micellar nanoparticle formulation, can extend in vivo antitumour activity and reduce the neurotoxicity of paclitaxel, Br. J. Cancer 92 (2005) 1240–1246.
[7] H. Uchino, Y. Matsumura, T. Negishi, F. Koizumi, T. Hayashi, T. Honda, N. Nishiyama, K. Kataoka, S. Naito, T. Kakizoe, Cisplatin-incorporating polymeric micelles (NC-6004) can reduce nephrotoxicity and neurotoxicity of cisplatin in rats, Br. J. Cancer 93 (2005) 678–687.
[8] Y. Matsumura, Preclinical and clinical studies of NK012, an SN-38-incorporating polymeric micelles, which is designed based on EPR effect, Adv. Drug Deliv. Rev. 63 (2011) 184–192.
[9] L. Helson, E. Okonkwo, L. Anton, E. Cvitkovic, cis-Platinum ototoxicity, Clin. Toxicol. 13 (1978) 469–478.
[10] R. Plummer, R.H. Wilson, H. Calvert, A.V. Boddy, M. Griffin, J. Sludden, M.J. Tilby, M. Eatock, D.G. Pearson, C.J. Ottley, Y. Matsumura, K. Kataoka, T. Nishiya, A Phase I clinical study of cisplatin-incorporated polymeric micelles (NC-6004) in patients with solid tumours, Br. J. Cancer 104 (2011) 593–598.
[11] N. Nishiyama, S. Okazaki, H. Cabral, M. Miyamoto, Y. Kato, Y. Sugiyama, K. Nishio, Y. Matsumura, K. Kataoka, Novel cisplatin-incorporated polymeric micelles can eradicate solid tumors in mice, Cancer Res. 63 (2003) 8977–8983.
[12] R.W. Fleischman, S.W. Stadnicki, M.F. Ethier, U. Schaeppi, Ototoxicity of cis-dichlorodiammine platinum (II) in the guinea pig, Toxicol. Appl. Pharmacol. 33 (1975) 320–332.
[13] L.P. Rybak, C.A. Whitworth, D. Mukherjea, V. Ramkumar, Mechanisms of cisplatin-induced ototoxicity and prevention, Hear. Res. 226 (2007) 157–167.
[14] A. Forge, L. Li, Apoptotic death of hair cells in mammalian vestibular sensory epithelia, Hear. Res. 139 (2000) 97–115.
[15] N. Dehne, J. Lautermann, F. Petrat, U. Rauen, H. de Groot, Cisplatin ototoxicity: involvement of iron and enhanced formation of superoxide anion radicals, Toxicol. Appl. Pharmacol. 174 (2001) 27–34.
[16] M. Wake, S. Takeno, D. Ibrahim, R. Harrison, Selective inner hair cell ototoxicity induced by carboplatin, Laryngoscope 104 (1994) 488–493.
[17] C.A. Rabik, M.E. Dolan, Molecular mechanisms of resistance and toxicity associated with platinating agents, Cancer Treat. Rev. 33 (2007) 9–23.
[18] J. Lokich, What is the "best" platinum: cisplatin, carboplatin, or oxaliplatin? Cancer Invest. 19 (2001) 756–760.
[19] W.C. Otto, R.D. Brown, L. Gage-White, S. Kupetz, M. Anniko, J.E. Penny, C.M. Henley, Effects of cisplatin and thiosulfate upon auditory brainstem responses of guinea pigs, Hear. Res. 35 (1988) 79–85.
[20] K.C. Campbell, L.P. Rybak, R.P. Meech, L. Hughes, D-methionine provides excellent protection from cisplatin ototoxicity in the rat, Hear. Res. 102 (1996) 90–98.
[21] D. Reser, M. Rho, D. Dewan, L. Herbst, G. Li, H. Stupak, K. Zur, J. Romaine, D. Frenz, L. Goldbloom, R. Kopke, J. Arezzo, T. Van De Water, L- and D-methionine provide equivalent long term protection against CDDP-induced ototoxicity in vivo, with partial in vitro and in vivo retention of antineoplastic activity, Neurotoxicology 20 (1999) 731–748.
[22] M.W. Church, J.A. Kaltenbach, B.W. Blakley, D.L. Burgio, The comparative effects of sodium thiosulfate, diethyldithiocarbamate, fosfomycin and WR-2721 on ameliorating cisplatin-induced ototoxicity, Hear. Res. 86 (1995) 195–203.

[23] L.P. Rybak, K. Husain, C. Morris, C. Whitworth, S. Somani, Effect of protective agents against cisplatin ototoxicity, Am. J. Otol. 21 (2000) 513–520.
[24] L.P. Rybak, K. Husain, C. Whitworth, S.M. Somani, Dose dependent protection by lipoic acid against cisplatin-induced ototoxicity in rats: antioxidant defense system, Toxicol. Sci. 47 (1999) 195–202.
[25] D. Thomas Dickey, L.L. Muldoon, D.F. Kraemer, E.A. Neuwelt, Protection against cisplatin-induced ototoxicity by N-acetylcysteine in a rat model, Hear. Res. 193 (2004) 25–30.
[26] M.S. Ford, S.B. Maggirwar, L.P. Rybak, C. Whitworth, V. Ramkumar, Expression and function of adenosine receptors in the chinchilla cochlea, Hear. Res. 105 (1997) 130–140.
[27] C.A. Whitworth, V. Ramkumar, B. Jones, N. Tsukasaki, L.P. Rybak, Protection against cisplatin ototoxicity by adenosine agonists, Biochem. Pharmacol. 67 (2004) 1801–1807.
[28] E.D. Lynch, R. Gu, C. Pierce, J. Kil, Combined oral delivery of ebselen and allopurinol reduces multiple cisplatin toxicities in rat breast and ovarian cancer models while enhancing anti-tumor activity, Anticancer Drugs 16 (2005) 569–579.
[29] M. Drottar, M.C. Liberman, R.R. Ratan, D.W. Roberson, The histone deacetylase inhibitor sodium butyrate protects against cisplatin-induced hearing loss in guinea pigs, Laryngoscope 116 (2006) 292–296.
[30] G. Li, S.H. Sha, E. Zotova, J. Arezzo, T. Van de Water, J. Schacht, Salicylate protects hearing and kidney function from cisplatin toxicity without compromising its oncolytic action, Lab Invest. 82 (2002) 585–596.
[31] G.W. Hill, D.K. Morest, K. Parham, Cisplatin-induced ototoxicity: effect of intratympanic dexamethasone injections, Otol. Neurotol. 29 (2008) 1005–1011.
[32] V. Hellberg, I. Wallin, S. Eriksson, E. Hernlund, E. Jerremalm, M. Berndtsson, S. Eksborg, E.S. Arnér, M. Shoshan, H. Ehrsson, G. Laurell, Cisplatin and oxaliplatin toxicity: importance of cochlear kinetics as a determinant for ototoxicity, J. Natl. Cancer Inst. 101 (2009) 37–47.
[33] S.S. Spicer, B.A. Schulte, Novel structures in marginal and intermediate cells presumably relate to functions of apical versus basal strial strata, Hear. Res. 200 (2005) 87–101.
[34] H. Hibino, Y. Kurachi, Molecular and physiological bases of the K+ circulation in the mammalian inner ear, Physiology (Bethesda) 21 (2006) 336–345.
[35] R. Ramírez-Camacho, D.E. Fernández, J.M. Verdaguer, M.M. Gómez, A. Trinidad, J.R. García-Berrocal, M.A. Corvillo, Cisplatin-induced hearing loss does not correlate with intracellular platinum concentration, Acta Otolaryngol. 128 (2008) 505–509.
[36] M.W. van Ruijven, J.C. de Groot, F. Hendriksen, G.F. Smoorenburg, Immunohistochemical detection of platinated DNA in the cochlea of cisplatin-treated guinea pigs, Hear. Res. 203 (2005) 112–121.
[37] J.W. Sepmeijer, S.F. Klis, Distribution of platinum in blood and perilymph in relation to cisplatin induced ototoxicity in the guinea pig, Hear. Res. 247 (2009) 34–39.
[38] C. Lanvers-Kaminsky, B. Krefeld, A.G. Dinnesen, D. Deuster, E. Seifert, G. Würthwein, U. Jaehde, A.C. Pieck, J. Boos, Continuous or repeated prolonged cisplatin infusions in children: a prospective study on ototoxicity, platinum concentrations, and standard serum parameters, Pediatr. Blood Cancer 47 (2006) 183–193.

Journal of Controlled Release 151 (2011) 104–109

Contents lists available at ScienceDirect

Journal of Controlled Release

journal homepage: www.elsevier.com/locate/jconrel

Concept Paper

In situ quantitative monitoring of polyplexes and polyplex micelles in the blood circulation using intravital real-time confocal laser scanning microscopy

Takahiro Nomoto [a,1], Yu Matsumoto [b,c,d,1], Kanjiro Miyata [b], Makoto Oba [e], Shigeto Fukushima [f], Nobuhiro Nishiyama [b], Tatsuya Yamasoba [c], Kazunori Kataoka [a,b,f,*]

[a] Department of Bioengineering, Graduate School of Engineering, The University of Tokyo, Japan
[b] Division of Clinical Biotechnology, Center for Disease Biology and Integrative Medicine, Graduate School of Medicine, The University of Tokyo, Japan
[c] Department of Otorhinolaryngology and Head and Neck Surgery, Graduate School of Medicine and Faculty of Medicine, The University of Tokyo, Japan
[d] Department of Otorhinolaryngology and Head and Neck Surgery, Mitsui Memorial Hospital, Japan
[e] Department of Vascular Regeneration, Division of Tissue Engineering, The University of Tokyo Hospital, Japan
[f] Department of Materials Engineering, Graduate School of Engineering, The University of Tokyo, Japan

ARTICLE INFO

Article history:
Received 12 January 2011
Accepted 10 February 2011
Available online 3 March 2011

Keywords:
Intravital confocal microscopy
Polyplex
Polyethylene glycol
Block copolymer
Polymer micelle

ABSTRACT

Surface modification using poly(ethylene glycol) (PEG) is a widely used strategy to improve the biocompatibility of cationic polymer-based nonviral gene vectors (polyplexes). A novel method based on intravital real-time confocal laser scanning microscopy (IVRTCLSM) was applied to quantify the dynamic states of polyplexes in the bloodstream, thereby demonstrating the efficacy of PEGylation to prevent their agglomeration. Blood flow in the earlobe blood vessels of experimental animals was monitored in a noninvasive manner to directly observe polyplexes in the circulation. Polyplexes formed distinct aggregates immediately after intravenous injection, followed by interaction with platelets. To quantify aggregate formation and platelet interaction, the coefficient of variation and Pearson's correlation coefficient were adopted. In contrast, polyplex micelles prepared through self-assembly of plasmid DNA with PEG-based block catiomers had dense PEG palisades, revealing no formation of aggregates without visible interaction with platelets during circulation. This is the first report of *in situ* monitoring and quantification of the availability of PEGylation to prevent polyplexes from agglomeration over time in the blood circulation. This shows the high utility of IVRTCLSM in drug and gene delivery research.

1. Concept of new methodologies

Gene therapy offers a unique potential for the treatment of genetic and intractable diseases and for tissue engineering. Its success is dependent upon the development of useful gene vectors as well as application of a drug delivery system (DDS). Nonviral gene vectors are attractive alternatives to viral gene vectors because they are much simpler to produce, transport and store, and induce fewer immune responses. Cationic polymers that electrostatically interact with plasmid DNA (pDNA) have been widely studied as materials to construct nonviral gene vectors [1–5]. The cationic polymers most commonly used as gene vectors include branched polyethylenimine (BPEI), linear polyethylenimine, poly(L-lysine) (PLys), chitosan, and dendrimers [6]. These polymers form polyion complexes (polyplexes) with pDNA to successfully transfer it into cultured cells to induce appreciable level of gene expression. However, these polyplexes have biocompatibility problems for systemic application. Polyplexes usually require excess polycations to generate electrostatic repulsion for their increased solubility and colloidal stability. This eventually results in a shift of their surface charge to a positive value. This positive charge causes nonspecific interaction with anionic components in the body such as plasma proteins and blood cells, which might lead to severe adverse effects [7,8]. Attachment of hydrophilic polymers such as poly(ethylene glycol) (PEG) is called "PEGylation" and has often been used to shield nonviral gene vectors from undesired interaction in the blood. PEGylation also contributes to diminished uptake by the reticuloendothelial system or macrophages, and hence the half-life in blood circulation can be extended.

It is well documented that a PEG palisade prevents nonspecific interaction with biological components. However, *in situ* evaluation of

Abbreviations: PEG, poly(ethylene glycol); DDS, drug delivery system; pDNA, plasmid DNA; BPEI, branched polyethylenimine; PLys, poly(L-lysine); PEG-PLys, poly(ethylene glycol)-*b*-poly(L-lysine); PAsp(DET), poly[*N*-[*N*-(2-aminoethyl)-2-aminoethyl]aspartamide]; PEG-PAsp(DET), poly(ethylene glycol)-*b*-poly[*N*-[*N*-(2-aminoethyl)-2-aminoethyl] aspartamide]; IVRTCLSM, intravital real-time confocal laser scanning microscopy; CV, coefficient of variation; PCC, Pearson's correlation coefficient.

* Corresponding author at: Department of Materials Engineering, Graduate School of Engineering, The University of Tokyo, 7-3-1 Hongo, Bunkyo-ku, Tokyo 113-0033, Japan. Tel.: +81 3 5841 7138; fax: +81 3 5841 7139.
E-mail address: kataoka@bmw.t.u-tokyo.ac.jp (K. Kataoka).

[1] These authors equally contributed to this work.

0168-3659/$ – see front matter © 2011 Elsevier B.V. All rights reserved.
doi:10.1016/j.jconrel.2011.02.011

the interaction between nonviral gene vectors and biological components has not been reported due to the absence of methodology to quantify the interaction. We recently described a method of direct and instantaneous observation of intravenously injected substances using intravital real-time confocal laser scanning microscopy (IVRTCLSM) [9]. IVRTCLSM provides high-speed scanning and simultaneous capture of multicolor fluorescence. The macromolecular agents flowing in the bloodstream in tumors, kidneys, and livers can be monitored using IVRTCLSM.

In the present study, we applied IVRTCLSM for the investigation of the interaction between nonviral gene vectors and biological components *in situ*. For the PEGylated polyplexes, we focused on polyplex micelles made through the self-assembly of pDNA with PEG-based cationic block copolymers [10–12]. We further developed an analytical methodology to quantify the dynamic states of nonviral gene vectors circulating in the bloodstream. This is the first report visualizing and quantifying the interaction between nonviral gene vectors and biological components over time and in real-time *in situ*.

2. Experimental methods

2.1. Sample preparation

Sterile Hepes (1 M, pH 7.3) was purchased from Amresco (Solon, OH, USA) and used as a buffer solution after dilution with distilled water. pDNA encoding the soluble form of vascular endothelial growth factor receptor-1 was labeled with Cy5 using Label IT Tracker Nucleic Acid Localization Kits (Mirus Bio Corporation, Madison, WI, USA). BPEI (molecular weight (MW) 22 kDa; Sigma-Aldrich, St. Louis, MO, USA) was dialyzed in 0.01 M HCl and lyophilized as a hydrochloride salt. BPEI and PLys (hydrobromide salt, MW 4–15 kDa; Sigma-Aldrich) were mixed with Cy5-labeled pDNA (150 μg/mL) at an N/P ratio of 6 and 2, respectively, to form polyplexes. The N/P ratio was defined as the residual molar ratio of amino groups of cationic segment to phosphate groups of pDNA. Poly{*N*-[*N*-(2-aminoethyl)-2-aminoethyl]aspartamide} (PAsp(DET)) (polymerization degree: 95) was synthesized as described previously [13]. PAsp(DET) was mixed with Cy5-labeled pDNA at an N/P ratio of 4. Poly(ethylene glycol)-*b*-poly(L-lysine) (PEG-PLys; MW of PEG: 12,000; polymerization degree of PLys segment: 45) was synthesized as described previously [14]. Poly(ethylene glycol)-*b*-poly{*N*-[*N*-(2-aminoethyl)-2-aminoethyl]aspartamide} (PEG-PAsp(DET); MW of PEG: 12,000 Da; polymerization degree of PAsp(DET) segment: 93) was synthesized by the aminolysis of PEG-poly(β-benzyl L-aspartate) block copolymer with diethylenetriamine according to a previous report [13]. PEG-PLys/pDNA and PEG-PAsp(DET)/pDNA micelles were prepared at an N/P ratio of 2 and 4, respectively. The final Cy5-labeled pDNA concentration was adjusted to 100 μg/mL in 10 mM Hepes buffer (pH 7.3).

2.2. Animal preparation

All animal experimental procedures were executed in accordance with the Guide for the Care and Use of Laboratory Animals as stated by the National Institutes of Health. Balb/c nude mice (female; Charles River Laboratories, Tokyo, Japan) were anesthetized with 3.0%–4.0% isoflurane (Abbott Japan Co., Ltd., Tokyo, Japan) using a Univenter 400 Anaesthesia Unit (Univentor Ltd., Zejtun, Malta). Mice were then subjected to lateral tail vein catheterization with a 30-gauge needle (Dentronics Co., Ltd., Tokyo, Japan) connected to a nontoxic, medical grade polyethylene tube (Natsume Seisakusho Co., Ltd., Tokyo, Japan). Platelets were labeled *in vivo* with the intravenous injection of DyLight 488-conjugated anti-GPIbβ antibody (X488; EMFRET Analytics, Eibelstadt, Germany) following the manufacturer's instructions. Mice were placed onto a custom-designed temperature-controlled microscope stage. The ear lobe was attached beneath the cover slip with a single drop of immersion oil as described in our previous report [9]. Video acquisition of the dermis tissue at a speed of 30 frames per second was performed for 10 min. Two-hundred microliters of naked pDNA, polyplexes, and micelles (20 μg of pDNA) were administered via the tail vein catheter 10 s after video acquisition was initiated. For the platelet inhibition study, 300 μL of aspirin (acetylsalicylic acid; Sigma-Aldrich) saturated aqueous solution was orally administered to mice for 2 consecutive days before IVRTCLSM.

2.3. IVRTCLSM imaging and processing

All picture/movie acquisitions were performed using a Nikon A1R confocal laser scanning microscope system attached to an upright ECLIPSE FN1 machine equipped with a CFI Apo 40× WI λS objective lens (Nikon, Tokyo, Japan). All pictures/movies were acquired at a scale of 79.55 μm × 79.55 μm with 5.11 μm of confocal slice. Acquired data were further processed using Nikon NIS Elements software. The region of interest (ROI) was manually defined in the vein. Image frames were extracted every 5 s from the video data for further analyses. For quantification of aggregates, the coefficient of variation (CV) of Cy5 fluorescence was calculated. For the platelet interaction study, colocalization between DyLight and Cy5 was evaluated by Pearson's correlation coefficient (PCC) [15]. All obtained values were plotted against time.

3. Discovery

3.1. Real-time observation of aggregates

We prepared BPEI/pDNA (N/P = 6), PLys/pDNA (N/P = 2), and PAsp (DET)/pDNA (N/P = 4) polyplexes as well as PEG-PLys/pDNA (N/P = 2) and PEG-PAsp(DET)/pDNA (N/P = 4) micelles. BPEI/pDNA was used as the representative polyplex containing excessive polycations. N/P ratios of PLys/pDNA and PAsp(DET)/pDNA were determined as the critical ratio to condense pDNA according to our previous report [16]. N/P ratios of PEG-PLys/pDNA and PEG-PAsp(DET)/pDNA micelles were determined at the same N/P ratios of PLys/pDNA and PAsp(DET)/pDNA polyplexes, respectively. The size and zeta potentials of these polyplexes and polyplex micelles were summarized in Supplementary Table 1.

Intravenously injected polyplexes and micelles were directly observed by IVRTCLSM. These dynamic states in the bloodstream were compared (Supplementary Videos 1–5). Extracted movie frames at indicated time points are shown in Fig. 1. Immediately after the BPEI/pDNA polyplex was injected, the fluorescence of Cy5 agglomerated into clumps with a variable size in several micrometers range. This nonuniform fluorescence distribution of the polyplex indicated formation of aggregates. PLys/pDNA and PAsp(DET)/pDNA polyplexes showed similar aggregate formation. In contrast, the fluorescence of Cy5 showed uniform distribution when PEG-PLys/pDNA and PEG-PAsp(DET)/pDNA micelles were injected, indicating the absence of aggregates.

3.2. Quantification of aggregates

Using the mean intensity of Cy5 fluorescence, the amount of Cy5-labeled pDNA was evaluated. We acquired the images every 5 s, calculated the relative fluorescence intensity defined as (Cy5 mean fluorescence intensity - Cy5 minimum fluorescence intensity)/(Cy5 maximum fluorescence intensity − Cy5 minimum fluorescence intensity), and plotted the relative fluorescence intensities against time. (Supplementary Fig. 1) The relative fluorescence intensities of naked pDNA decreased immediately, and almost disappeared within 5 min after the start of acquisition. The relative fluorescence intensities of BPEI/pDNA, PLys/pDNA, and PAsp(DET)/pDNA polyplexes also rapidly decreased and dropped to around 0.2 within 10 min after the start of acquisition. In contrast, PEG-PLys/pDNA, and PEG-PAsp(DET)/pDNA polyplex micelles maintained the relative

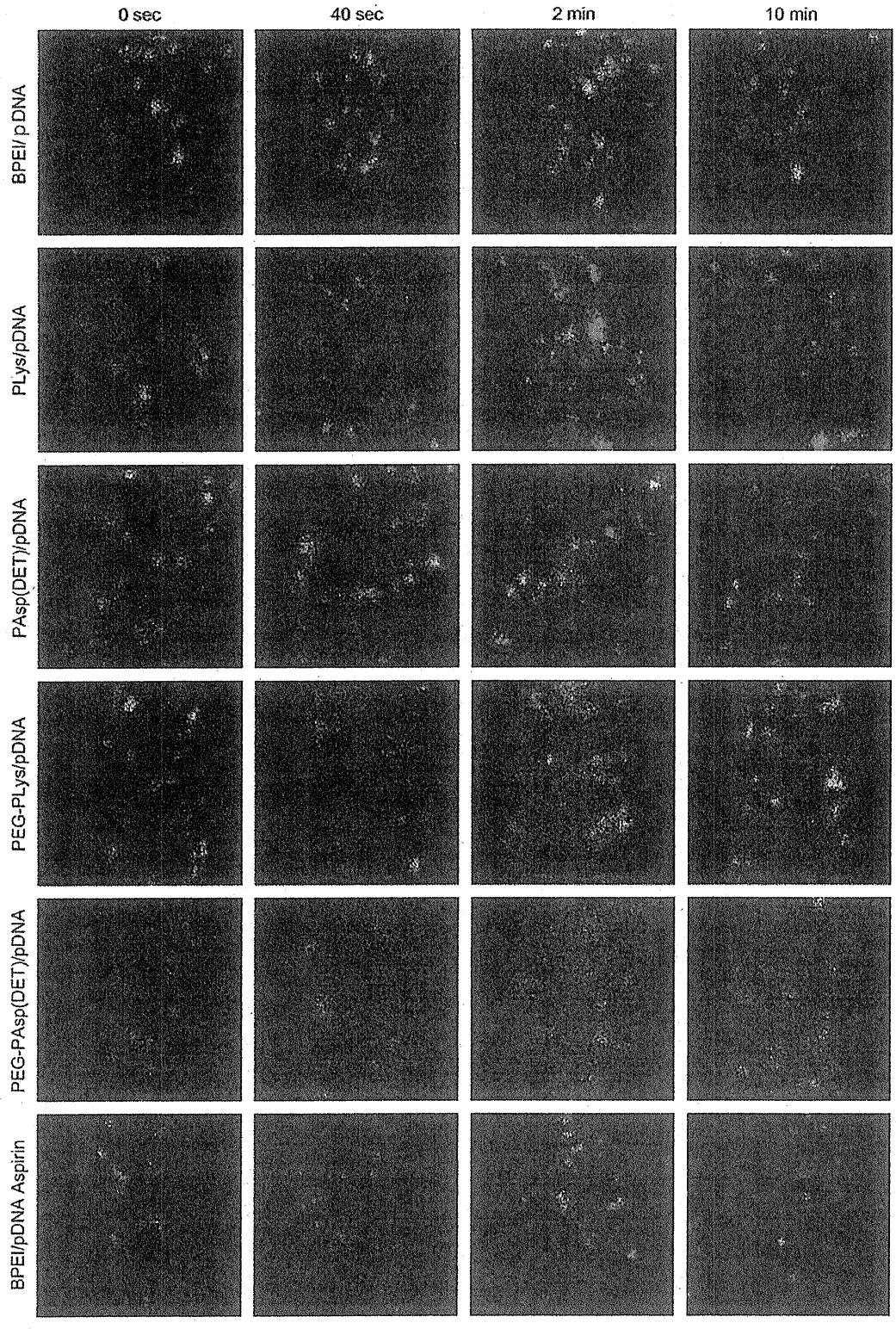

Fig. 1. Intravital confocal micro-videography of polyplexes and polyplex micelles in the bloodstream of the mouse earlobe. Prior to observation, the anti-GPIbβ antibody conjugated with DyLight 488 was injected to label platelets (green). The polyplexes and polyplex micelles incorporating Cy5-labeled pDNA (red) were intravenously injected 10 s after start of observation. Image frames were extracted from videos at identical time points for comparison. Image size: 79.55 μm × 79.55 μm. Confocal slice: 5.11 μm.

fluorescence intensities of around 0.9 and 0.7 even 10 min after the start of acquisition, suggesting the prolonged blood circulation. These results are consistent with the previous studies, which demonstrated pDNA degradation within 5 min and the improvement of blood circulation by PEGylation [17,18].

However, the relative fluorescence intensities could not provide the information about the aggregates of polyplexes and polyplex micelles. Thus, the quantification of aggregates was performed by CV calculation of Cy5 fluorescence in the ROI. The CV is a normalized measure of dispersion of a distribution, and is defined as the ratio of

the standard deviation to the mean. We acquired the images every 5 s, calculated the CV, and plotted the CV against time (Fig. 2). CV values of the polyplexes rapidly increased upon first entry into the vein of the earlobe immediately after intravenous injection. CV values of the polyplexes subsequently fluctuated and decreased over time. In contrast, CV values of the micelles slightly increased upon first entry due to the admixture of micelles and blood, and remained at a plateau at the lower values without fluctuation.

3.3. Platelet interaction study

Platelet is known to be the primary cell components involved in the initial event of thrombosis, and polycations initiate the process of platelet clots formation [19–21]. Thus, in this study, we focused on platelets interaction with cationic polyplexes. To investigate the interaction of polyplexes with platelets, we labeled platelets with DyLight 488-conjugated anti-GPIbβ antibody, and observed the interaction using IVRTCLSM (Fig. 1, Supplementary Videos 1–5). The average labeling efficiency of the antibody has been reported to be ~90% [22]. BPEI/pDNA, PLys/pDNA, and PAsp(DET)/pDNA polyplexes formed aggregates immediately after injection as described above. Their adhesion to platelets was clearly observed approximately 2 min after injection as judged from the colocalization of red and green fluorescences to appear as yellow colored pixels. In contrast, PEG-PLys/pDNA and PEG-PAsp(DET)/pDNA micelles showed no adhesion to platelets throughout the whole experiment.

3.4. Platelet interaction quantification

To quantify the interaction between polyplexes and platelets, we acquired the images every 5 s, and calculated the colocalization between Cy5 fluorescence and DyLight 488 fluorescence using PCC [15]. PCC indicates the intensity of the correlation of two elements, ranging from −1 to +1. The PCC value of the BPEI/pDNA polyplex fluctuated and increased up to approximately 0.4 (Fig. 3). PLys/pDNA and PAsp(DET)/pDNA polyplexes also fluctuated and increased up to approximately 0.25 and 0.33, respectively. In contrast, PCC values of PEG-PLys/pDNA and PEG-PAsp(DET)/pDNA micelles were maintained at almost zero throughout the study.

3.5. Platelet inhibition study

To investigate whether inhibition of platelet function decreases aggregates formation, aspirin was used as an anti-platelet agent. We compared the CV and PCC of the BPEI/pDNA polyplex between aspirin-administered mice and nonadministered control mice (Figs. 1 and 4, Supplementary Video 6). The CV value of the aspirin-administered mice was almost identical to that of control mice; however, their PCC value remained <0.1 throughout the study.

4. Interpretation and significance of new methodologies

Pharmacokinetic studies are indispensable for developing efficient DDSs that transport drugs specifically to the targeted tissue. Pharmacokinetic studies using animals have primarily relied on *ex vivo* techniques, such as analyzing blood or urine samples. These *ex vivo* techniques have been well established to analyze blood circulation, target accumulation, or other pharmacological information of the DDS. However, this approach provides only static information at specific time points. Therefore, investigating dynamic and longitudinal events using this approach is difficult. Alternatively, the intravital microscopy is an emerging technique [23], allowing to investigate such dynamic states of DDS in animals. Recently, we developed the intravital microscopy equipped with fast-scanning laser confocal systems (IVRTCLSM) [9], and demonstrated here its application as a novel tool to dynamically evaluate the interaction between gene vectors and blood components. Our method is characterized by noninvasive observation with high spatial and temporal resolutions to quantitatively monitor the dynamic states

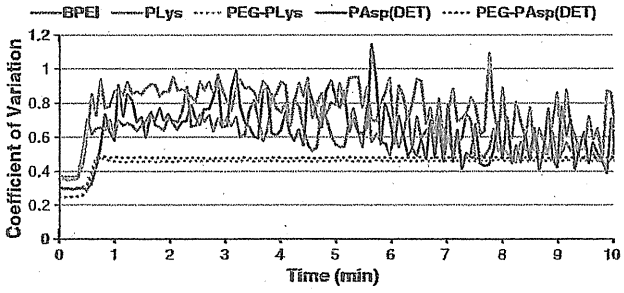

Fig. 2. Quantification of aggregates of polyplexes and micelles. Aggregates of polyplexes and micelles were quantified with CV of Cy5 fluorescence intensities in the frames extracted every 5 s from crude videos.

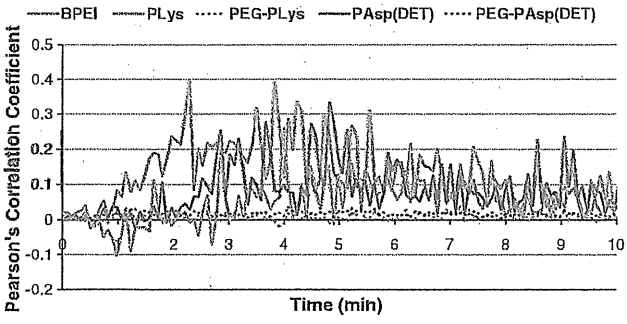

Fig. 3. Quantification of colocalization between polyplexes/micelles and platelets. The colocalization was measured with PCC. PCC was calculated from the frames extracted every 5 s from crude videos.

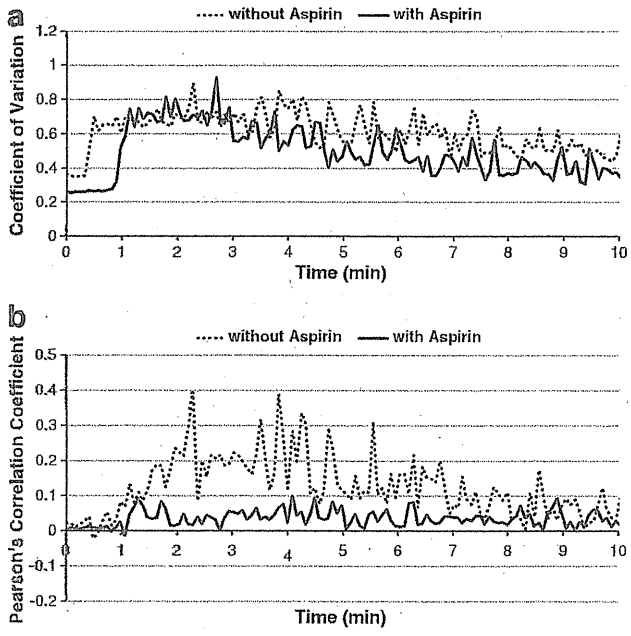

Fig. 4. Platelets inhibition study with aspirin. (a) Aggregates of BPEI/pDNA polyplexes of the aspirin-administered mouse was quantified with the CV of Cy5 fluorescence intensities in the frames extracted every 5 s from crude videos. (b) Colocalization between BPEI/pDNA polyplexes and platelets of the aspirin-administered mouse was quantified with PCC. PCC was calculated from the frames extracted every 5 s from crude videos. For comparison, the CV and PCC of the BPEI/pDNA polyplexes-administered normal mouse in Figs. 2 and 3 were shown respectively again.

of nonviral gene vectors. In the present study, the mouse earlobe was noninvasively fixed beneath the coverslip, and the vein was imaged at the dermis layer. Confocal imaging eliminated light from out-of-focus sections in the ear lobe such as the epidermis and hypodermis. Furthermore, we kept the confocal slice thinner (5.11 μm) than the diameter of the vein, so that the signal was detected only from inside the vasculature. High-speed scanning was essential to obtain unambiguous images to quantify the aggregates and colocalization between nonviral gene vectors and platelets because conventional galvano scanners are too slow to distinguish the individual aggregates and platelets rapidly flowing in the bloodstream, providing insufficient and blurred images (Supplementary Videos 7 and 8).

We investigated the polycations BPEI and PLys. They are widely used to construct polyplexes and PAsp(DET) has reduced cytotoxicity and high transfection efficiency [13]. To evaluate the improvement of biocompatibility via PEGylation, PEG-PLys/pDNA and PEG-PAsp (DET)/pDNA micelles were examined. A simple and effective way to PEGylate polyplexes is, as we reported [10–12], to use PEG-based cationic block copolymers as counterpart polycations to pDNA. The block copolymers are characterized by tandem alignment of a hydrophilic PEG segment and a cationic segment, leading to the formation of stable and biocompatible micelles with a core of polycation/pDNA complex surrounded by a dense PEG palisade and size of approximately 100 nm. Indeed, the micelle composed of PEG-PLys and pDNA achieved higher stability than that of unmodified PLys/pDNA polyplex in a medium containing serum and showed prolonged blood circulation [18,24]. The block copolymer possessing a cationic polyaspartamide segment carrying an ethylenediamine unit at the side chain, PEG-PAsp(DET), also formed the micelle with pDNA, which prevented nonspecific interaction with biological components such as erythrocytes and platelets under *in vitro* conditions [8].

IVRTCLSM was used to directly investigate the interaction between these gene vectors and platelets in the bloodstream. IVRTCLSM could be used to evaluate the dynamic states of nonviral gene vectors rapidly flowing in the bloodstream over time *in situ* (Fig. 1 and Supplementary Videos 1–6). This is the first report to visualize the formation of aggregates and the prevention by PEGlyation of polyplexes *in situ* in the bloodstream.

To quantify the aggregates, we adopted the CV. CV values reflected the nonuniform fluorescence distribution of polyplexes and uniform fluorescence distribution of micelles (Fig. 2). It is noteworthy that our IVRTCLSM started video acquisition 10 s before administration, allowing us to follow aggregate formation immediately after injection. CV values of the polyplexes rapidly increased approximately 20–30 s after injection, and corresponded well with the entry of polyplexes, indicating instantaneous formation of aggregates (Fig. 2). CV values also fluctuated over time, depending on the amount of aggregates at those time points. Furthermore, CV values of polyplexes decreased with time due to their disappearance from the bloodstream. In contrast, CV values of micelles were moderately elevated when micelles passed the ROI first. This moderate elevation was because of the admixture of micelles and blood without aggregate formation. Moreover, CV values were retained at a plateau after this moderate elevation, suggesting persistent circulation and uniform distribution of micelles in the bloodstream.

IVRTCLSM was also useful for the investigation of the dynamic interaction between nonviral gene vectors and platelets. Indeed, we succeeded in visualizing the interaction between polyplexes and platelets *in situ*. This dynamic information could not be revealed without IVRTCLSM.

To quantify the platelet interaction, we adopted PCC between polyplexes/micelles and platelets (Fig. 3). PCC values of polyplexes did not increase at the time point when CV values started to increase. PCC values began to increase after approximately 1 min after injection, and indicated strong correlation between polyplexes and platelets 2 min after injection. This temporal gap between aggregate formation and platelet interaction strongly indicated that aggregate formation was not triggered by platelets. To confirm this, we conducted the study in mice that were administered aspirin (Fig. 4). Aspirin induces a long-lasting functional defect in platelets [25], and thus may inhibit platelet interaction with polyplexes. The CV and PCC quantitatively demonstrated that oral administration of aspirin successfully inhibited platelet interaction with aggregates (Fig. 4b), but did not inhibit aggregate formation itself (Fig. 4a). This result indicates that the aggregate formation of polyplexes does not involve platelets (at least in the initial stage). Presumably, some protein components in plasma may have a role in aggregate formation, but further investigation is needed to clarify the mechanism.

Aggregate formation in the range of several micrometers immediately after intravenous injection should crucially affect the efficiency of systemically injected polyplexes. The aggregated polyplexes cannot extravasate into the targeted tissues or cells. Moreover, they might lead to thrombosis through the interaction with platelets to obstruct microvessels in normal tissue, including the lungs and liver, resulting in nonspecific accumulation of polyplexes in these tissues. This accumulation caused by aggregate formation will lead to unfavorable effects such as pulmonary embolism. The micelles, in contrast, did not form aggregates, and also showed no interaction with platelets. Thus, they are expected to prevent adverse effects caused by polyplex agglomeration, which cannot be inhibited even by oral administration of aspirin. This result confirms that PEGylation is a rational strategy to improve the biocompatibility of nonviral gene vectors based on polyplex formation [3,10–12].

In the present study, IVRTCLSM was used to visualize and quantify the dynamic states of polyplexes flowing in the bloodstream. Moreover, with respect to ethics, IVRTCLSM excels conventional *ex vivo* methods that involve the sacrifices of numerous animals to acquire pharmacokinetic information. IVRTCLSM provides temporal and spatial information at 30 time points in 1 s with a single mouse, which is desirable for high-throughput screening of newly developed DDSs.

In conclusion, IVRTCLSM was developed and applied to directly investigate the dynamic state of gene vectors in the bloodstream. Aggregate formation of the polyplexes and its prevention by PEGylation was observed *in situ* for the first time under the flow in the capillary. Thus, IVRTCLSM could provide the requisite information that has not been obtained by conventional methods, thereby giving a new facet in the research on systemic gene delivery.

Supplementary materials related to this article can be found online at doi:10.1016/j.jconrel.2011.02.011.

Acknowledgment

This work was supported in part by Core Research Program for Evolutional Science and Technology (CREST) from the Japan Science and Technology Corporation (JST) and Funding Program for World-Leading Innovative R&D on Science and Technology (FIRST Program) from Japan Society for the Promotion of Science (JSPS).

References

[1] D.W. Pack, A.S. Hoffman, S. Pun, P.S. Stayton, Design and development of polymers for gene delivery, Nat. Rev. Drug Discov. 4 (2005) 581–593.
[2] T. Merdan, K. Kunath, H. Petersen, U. Bakowsky, K.H. Voigt, J. Kopecek, T. Kissel, PEGylation of poly(ethylene imine) affects stability of complexes with plasmid DNA under in vivo conditions in a dose-dependent manner after intravenous injection into mice, Bioconjug. Chem. 16 (2005) 785–792.
[3] M. Ogris, E. Wagner, Targeting tumors with non-viral gene delivery systems, Drug Discov. Today 7 (2002) 479–485.
[4] Y. Kakizawa, K. Kataoka, Block copolymer micelles for delivery of gene and related compounds, Adv Drug Deliver Rev 54 (2002) 203–222.

[5] K. Osada, R.J. Christie, K. Kataoka, Polymeric micelles from poly(ethylene glycol)-poly(amino acid) block copolymer for drug and gene delivery, J. R. Soc. Interface 6 (2009) S325–S339.
[6] Y.Y. Yang, Y. Wang, R. Powell, P. Chan, Polymeric core–shell nanoparticles for therapeutics, Clin. Exp. Pharmacol. Physiol. 33 (2006) 557–562.
[7] M. Ogris, S. Brunner, S. Schuller, R. Kircheis, E. Wagner, PEGylated DNA/transferrin-PEI complexes: reduced interaction with blood components, extended circulation in blood and potential for systemic gene delivery, Gene Ther. 6 (1999) 595–605.
[8] D. Akagi, M. Oba, H. Koyama, N. Nishiyama, S. Fukushima, T. Miyata, H. Nagawa, K. Kataoka, Biocompatible micellar nanovectors achieve efficient gene transfer to vascular lesions without cytotoxicity and thrombus formation, Gene Ther. 14 (2007) 1029–1038.
[9] Y. Matsumoto, T. Nomoto, H. Cabral, Y. Matsumoto, S. Watanabe, R.J. Christie, K. Miyata, M. Oba, T. Ogura, Y. Yamasaki, N. Nishiyama, T. Yamasoba, K. Kataoka, Direct and instantaneous observation of intravenously injected substances using intravital confocal micro-videography, Biomed. Opt. Express 1 (2010) 1209–1216.
[10] K. Osada, R.J. Christie, K. Kataoka, Polymeric micelles from poly(ethylene glycol)-poly(amino acid) block copolymer for drug and gene delivery, J. R. Soc. Interface 6 (Suppl. 3) (2009) S325–339.
[11] Y. Kakizawa, K. Kataoka, Block copolymer micelles for delivery of gene and related compounds, Adv. Drug Deliv. Rev. 54 (2002) 203–222.
[12] N. Nishiyama, K. Kataoka, Current state, achievements, and future prospects of polymeric micelles as nanocarriers for drug and gene delivery, Pharmacol. Ther. 112 (2006) 630–648.
[13] K. Itaka, T. Ishii, Y. Hasegawa, K. Kataoka, Biodegradable polyamino acid-based polycations as safe and effective gene carrier minimizing cumulative toxicity, Biomaterials 31 (2010) 3707–3714.
[14] A. Harada, K. Kataoka, Formation of polyion complex micelles in an aqueous milieu from a pair of oppositely-charged block-copolymers with poly(ethylene glycol) segments, Macromolecules 28 (1995) 5294–5299.
[15] V. Zinchuk, O. Zinchuk, T. Okada, Quantitative colocalization analysis of multicolor confocal immunofluorescence microscopy images: pushing pixels to explore biological phenomena, Acta Histochem. Et Cytochem. 40 (2007) 101–111.
[16] K. Miyata, S. Fukushima, N. Nishiyama, Y. Yamasaki, K. Kataoka, PEG-based block catiomers possessing DNA anchoring and endosomal escaping functions to form polyplex micelles with improved stability and high transfection efficacy, J. Control. Release 122 (2007) 252–260.
[17] K. Kawabata, Y. Takakura, M. Hashida, The fate of plasmid dna after intravenous-injection in mice — involvement of scavenger receptors in its hepatic-uptake, Pharm. Res. 12 (1995) 825–830.
[18] M. Harada-Shiba, K. Yamauchi, A. Harada, I. Takamisawa, K. Shimokado, K. Kataoka, Polyion complex micelles as vectors in gene therapy — pharmacokinetics and in vivo gene transfer, Gene Ther. 9 (2002) 407–414.
[19] K. Kataoka, T. Tsuruta, T. Akaike, Y. Sakurai, Biomedical behavior of synthetic polyion complexes toward blood-platelets, Makromolekulare Chem. Macromol. Chem. Phys. 181 (1980) 1363–1373.
[20] T.K. Rosborough, Parallel inhibition of ristocetin and polycation-induced platelet agglutination, Thromb. Res. 19 (1980) 417–422.
[21] P. Chollet, M.C. Favrot, A. Hurbin, J.L. Coll, Side-effects of a systemic injection of linear polyethylenimine–DNA complexes, J. Gene Med. 4 (2002) 84–91.
[22] M.R. Dowling, E.C. Josefsson, K.J. Henley, P.D. Hodgkin, B.T. Kile, Platelet senescence is regulated by an internal timer, not damage inflicted by hits, Blood 116 (2010) 1776–1778.
[23] S. Hak, N.K. Reitan, O. Haraldseth, C. Lange Davies, Intravital microscopy in window chambers: a unique tool to study tumor angiogenesis and delivery of nanoparticles, Angiogenesis 13 (2010) 113–130.
[24] K. Itaka, K. Yamauchi, A. Harada, K. Nakamura, H. Kawaguchi, K. Kataoka, Polyion complex micelles from plasmid DNA and poly(ethylene glycol)-poly(L-lysine) block copolymer as serum-tolerable polyplex system: physicochemical properties of micelles relevant to gene transfection efficiency, Biomaterials 24 (2003) 4495–4506.
[25] C. Patrono, Aspirin as an antiplatelet drug, N. Engl. J. Med. 330 (1994) 1287–1294.

ELSEVIER

Auris Nasus Larynx 38 (2011) 638–642

AURIS NASUS LARYNX
INTERNATIONAL JOURNAL OF ORL & HNS

www.elsevier.com/locate/anl

Preservation of vestibular function after scala vestibuli cochlear implantation

Mitsuya Suzuki [a,*], Takio Goto [b], Akinori Kashio [b], Takuya Yasui [b], Takashi Sakamoto [b], Ken Ito [c], Tatsuya Yamasoba [b]

[a] *Department of Otolaryngology, Sakura Medical Center, University of Toho, Chiba 285-0841, Japan*
[b] *Department of Otolaryngology, University of Tokyo, Tokyo 133-8655, Japan*
[c] *Department of Otolaryngology, University of Teikyo, Tokyo 173-8606, Japan*

Received 6 June 2010; accepted 13 January 2011
Available online 16 February 2011

Abstract

A 58-year-old man, in whom the cochlear implant (CI) had been inserted into the left ear, had right middle-ear cancer. The CI was removed immediately before receiving subtotal removal of right temporal bone. Four months later, the CI was again inserted in his left cochlea. Because of obliterated scala tympani, the 22 active electrodes of the CI were placed into the scala vestibuli. After the surgery, the patient complained that he experienced rotary vertigo and "jumbling of vertical direction" of objects on walking. Using rotation test, we evaluated vestibular function of remaining left ear. Numerous horizontal nystagmus beats were induced during earth-vertical axis rotation, whereas vertical downbeat nystagmus was scarcely induced during off-vertical axis rotation. The horizontal vestibulo-ocular reflex (VOR) was almost normally induced by sinusoidal stimulation at 0.8 Hz. These data suggest that the scala vestibuli insertion of CI would be not so invasive against the lateral semicircular canal.

Keywords: CI; Scala vestibuli; Bilateral vestibular dysfunction; Lateral cranial base surgery

1. Introduction

Sensorineural hearing loss resulting from otosclerosis, meningitis, chronic otitis media or trauma can be associated with partial or total obstruction of the scala tympani [1,2]. Although cochlear implants are usually inserted into the scala tympani, the scala vestibuli might be chosen as an alternative implantation site in a case of obliterated scala tympani [3–5].

Although several investigators have reported the effectiveness of the implantation of a cochlear device into the scala vestibuli for recovering hearing function [3–5], few data are available regarding the effect of cochlear implantation on vestibular function. Although a few investigators have reported that no vestibular symptoms occurred after the insertion of CIs into the scala vestibuli, they did not demonstrate any neuro-otological tests such as the caloric response and rotational stimulation tests [3,5]. In the present study, we evaluated the we evaluated the residual vestibular function by studying eye movements induced by earth-vertical axis rotation (EVAR) and off-vertical axis rotation (OVAR), and the vestibule-ocular reflex (VOR) in a patient in whom a cochlear device had been inserted into the scala vestibule after receiving subtotal removal of opposite temporal bone.

2. Case report

A 58-year-old man had profound sensorineural hearing loss because of chronic otitis media. Because of the stenosis of the scala tympani owing to fibrosis, only 10 active

* Corresponding author. Tel.: +81 43 462 8811; fax: +81 43 462 8741.
E-mail address: misuzuki-tky@umin.ac.jp (M. Suzuki).

0385-8146/$ – see front matter
doi:10.1016/j.anl.2011.01.014

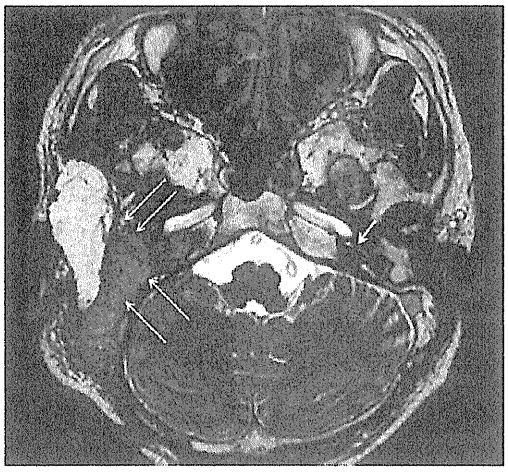

Fig. 1. MRI image at 4 months after right lateral cranial base surgery. The image shows a faint fluid intensity in the left cochlear basal turn. Long arrow: rectus abdominis musculocutaneous flap, short arrows: left cochlear basal turn.

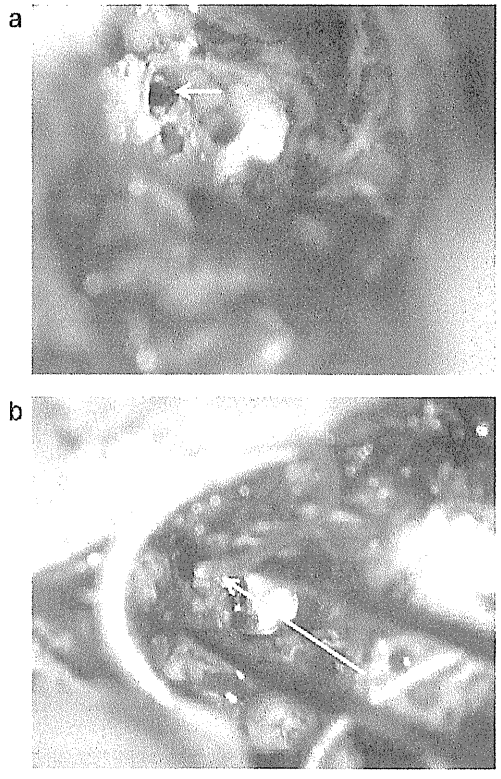

Fig. 2. The scala vestibuli is exposed, with no evidence of fibrosis, presence of scar tissue, or ossification. Short arrow: scala vestibule, long arrow: Nucleus 24 CI placed in the scala vestibuli.

electrodes of Nucleus 24 CI (CI) were inserted into the scala tympani of the left ear in early March 2001. After the surgery, he had neither dizziness nor vertigo. In late November 2007, subtotal removal of right temporal bone was planned of squamous cell carcinoma, which had infiltrated the external auditory canal from the middle ear. Because a radio-knife needs to be used during lateral cranial base surgery, the CI had to be removed. First, the CI was removed, and a polyethylene tube of the same size as the electrode was inserted instead of the electrode of the CI, and then, subtotal removal of right temporal bone was performed. The patient complained of rotary vertigo for 10 days after the surgery. Four months later, an MRI image showed no local recurrence of cancer and a faint fluid intensity in the left cochlear basal turn (Fig. 1). In late March 2008, the CI was reinserted into the left ear. After a skin incision was made, the mastoid cavity was exposed. While looking for the polyethylene tube, we found that it had naturally separated from the scala tympani. The small hole made on the lateral wall of the scala tympani was completely obliterated. Because of the obliteration of the scala tympani owing to fibrosis and the proliferation of scar tissue, we dissected the inferior and ascending segments of the basal turn to identify a lumen suitable for cochlear implantation, but were unable to find any. The scala vestibuli was then opened by drilling superior to the spiral ligament in the ascending segments. No evidence of fibrosis, scar tissue, or ossification was found in the scala vestibuli (Fig. 2(a) and (b)). All 22 active electrodes of the Nucleus 24 CI were successfully placed in the scala vestibuli around the modiolus. Spontaneous horizontal nystagmus to the left side was observed using Frenzel's glasses for 7 days after cochlear implantation. After a month of sound stimulation, his single syllable recognition score was 54% without visual cues and 70% with visual cues. For 3 months after the last surgery, he has been complained of "jumbling of vertical direction" of objects in his visual field when in motion. Caloric response and VEMP were not performed because of the obliteration of the external auditory canal. Bone-conducted VEMP was not performed because the patient did not give consent. Head thrust test could not be performed because the neck was stiff due to neck dissection.

We performed the unidirectional damped-rotation test as follows. The patient's head was inclined forward by 30°, and his horizontal and vertical eye movements induced by either EVAR or OVAR on a rotary axis tilted at 15° were recorded using electronystagmography (ENG), for which the time constant was set at 0.003 s. The maximal angular velocity increased up to 160°/s, and then it reduced at a rate of $-4°/s^2$. ENG revealed numerous horizontal nystagmus beats toward the left side during EVAR in the left direction and toward the right side during EVAR in the right direction. The number of horizontal nystagmus beats during EVAR in the left direction was similar to that during EVAR in the right direction (Fig. 3a). Numerous horizontal nystagmus beats was induced during OVAR in both directions, whereas vertical nystagmus was scarcely induced during OVAR in either direction (Fig. 3b).

The horizontal VOR was also recorded using ENG. The chair in which the subject was seated was first rotated to the

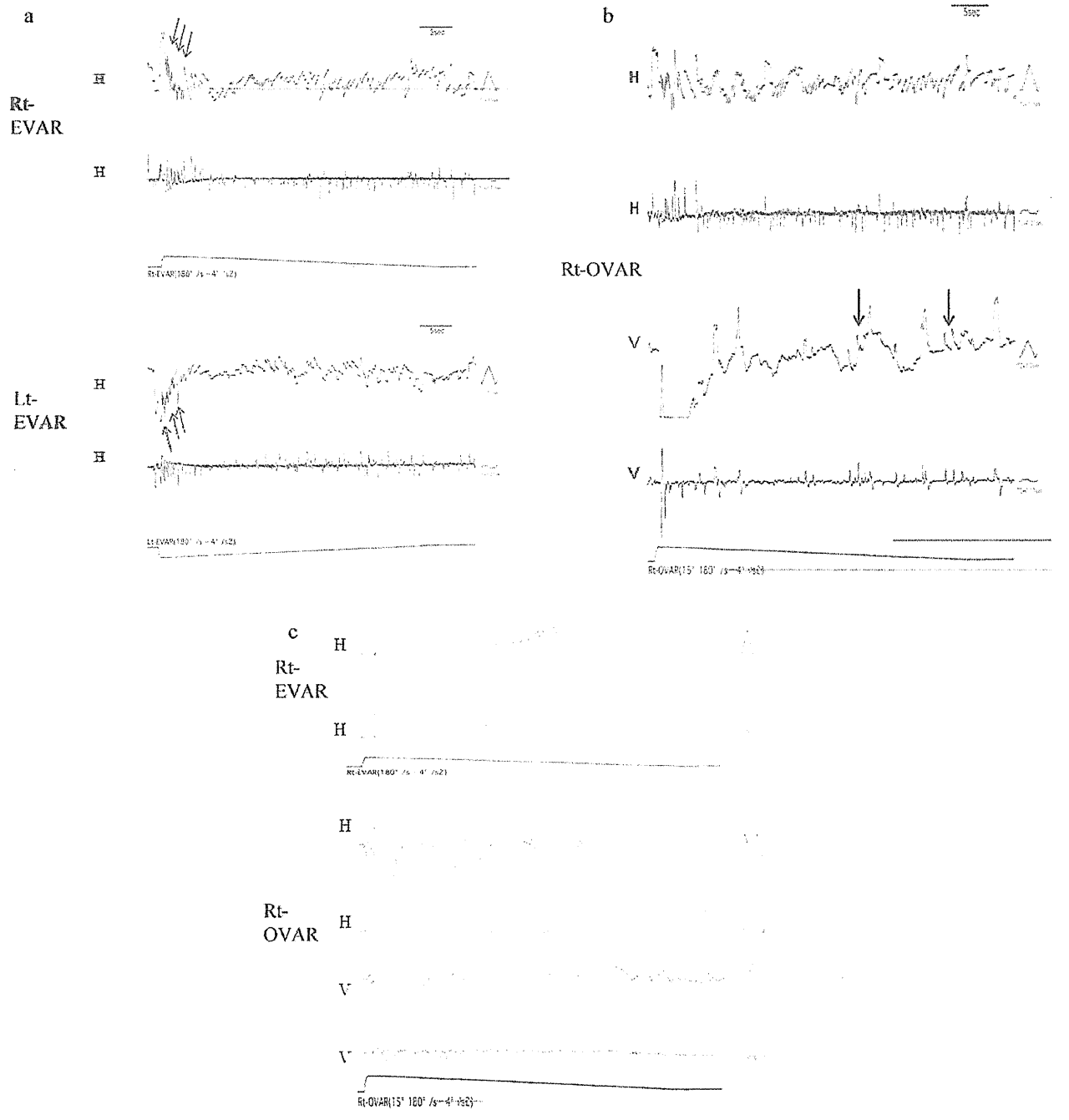

Fig. 3. (a) Horizontal eye movements (arrows) induced by either direction of EVAR. The number of horizontal nystagmus beats is similar during EVAR in either direction. (b) Horizontal and vertical eye movements induced by rt-OVAR. Numerous horizontal nystagmus is induced during OVAR. Vertical nystagmus is scarcely induced during OVAR. Arrows: vertical nystagmus. (c) rt-EVAR and rt-OVAR recorded in control subject.

right and left by 30° at 0.2, 0.6 and 0.8 Hz, while the subject was looking at a target placed 1 m ahead. Subsequently, the chair was rotated to the right and left by 30° at 0.2, 0.6 and 0.8 Hz while the subject recalled the position of the target in the dark. In the dark, horizontal VOR was not induced by horizontal sinusoidal stimulation at 0.2 Hz. VOR was induced by sinusoidal stimulation at 0.6 Hz; however, horizontal nystagmus to the right side was superimposed on the sinusoidal shape. During VOR induced by sinusoidal stimulation at 0.8 Hz, the eye movements showed a nearly normal shape (VOR gain = 0.8) (Fig. 4).

Twenty months later, his single syllable recognition score improved up to 70% without visual cues and up to 80% with visual cues. However, the horizontal and the vertical nystagmus beats during EVAR or OVAR did not change.

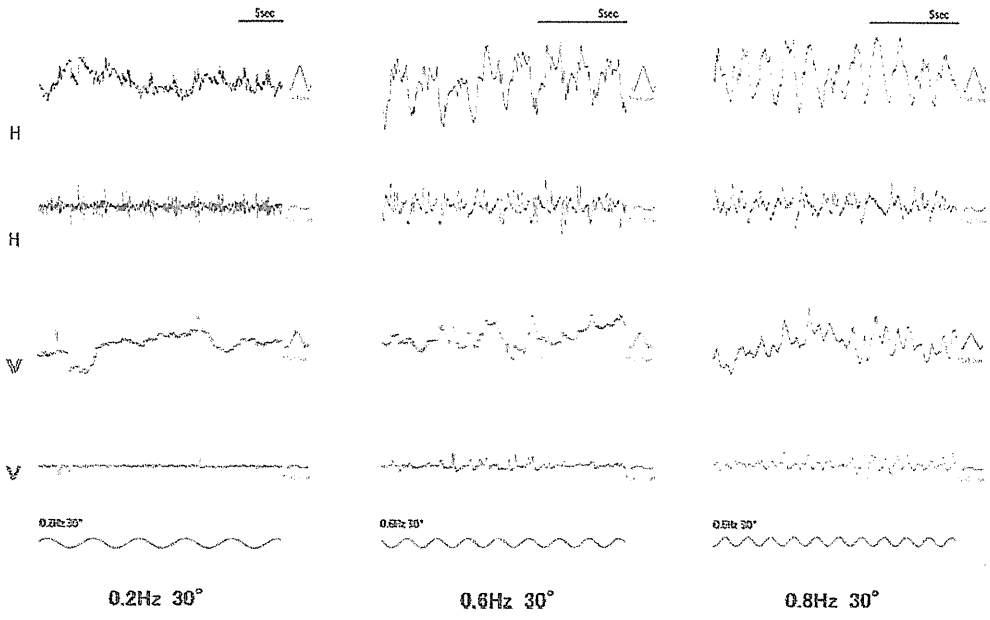

Fig. 4. VOR recorded using ENG with a vertical or horizontal inducement electrode. The horizontal VOR induced by sinusoidal stimulation at 0.8 Hz shows a nearly normal shape.

3. Discussion

In this study, we evaluated the vestibular function in a patient in whom a cochlear device had been inserted into the scala vestibuli of the left ear after subtotal removal of temporal bone had been performed in the opposite ear. Only vestibular functions in left ear were evaluated using eye movements induced by EVAR or OVAR, and using VOR induced by sinusoidal rotational movement. Thus, we identified that vestibular function was still preserved after a CI had been inserted into the scala vestibuli.

Cochlear ossification is not rare occurrence in patients who have undergone cochlear implantation. Histopathologic studies have revealed that the most common region of cochlear ossification, regardless of the etiology, is the basal turn of the scala tympani [6]. Although scala vestibuli ossification is rare occurence, it might be caused by chronic otitis media [6]. In the current case, since preoperative MRI images showed faint fluid intensity in the left cochlear basal turn, we suspected that the scala tympani and/or vestibuli of the basal turn had either been obliterated or had undergone stenosis. During surgery, we found that the scala tympani had indeed been obliterated; however, the scala vestibuli was found to be open without granulation tissue or fibrosis. In addition, the patient experienced rotary vertigo and spontaneous horizontal nystagmus for 7 days after the cochlear implant had been inserted into the scala vestibuli. These episodes suggest that the scala vestibuli in the basal turn is connected to the perilymphatic space in the vestibular labyrinth, and that the remaining vestibular function was irritated by the insertion of the CI into the scala vestibuli.

EVAR and OVAR are well-known rotational tests that simultaneously stimulate the vestibular labyrinth in both ears. In the current case, EVAR or OVAR were used to stimulate the vestibular labyrinth of which the CI had been inserted to the scala vestibule, because the contralateral labyrinth had been extirpated by subtotal removal of temporal bone. The number of horizontal nystagmus beats during EVAR or OVAR in the left direction was similar to that during EVAR or OVAR in the left direction, respectively. Takahashi et al. [7] reported that eye speed in the slow phase and the number of nystagmus beats induced by ampullopetal stimulation are both greater than those induced by ampullofugal stimulation in the lateral semicircular canal in monkeys. Several investigators have demonstrated that the number of nystagmus beats induced by EVAR may be asymmetrical in a patient with severe vestibular loss in both ears [7,8]. In the current case, numerous horizontal nystagmus beats during EVAR was induced by not only ampullopetal stimulation but also ampullofugal stimulation of the lateral semicircular canal. One possible explanation is that the function of the lateral semicircular canals may not be severely disturbed by the insertion of a CI into the scala vestibuli. Appropriate visual stimuli can adjust VOR gain in chickens treated with streptomycin [9]. Fetter et al. [10] have reported that visual experience plays an important role in the recovery of VOR after labyrinthectomy. Alternatively, vestibular compensation may lead to the recovery of VOR after subtotal removal of the right temporal bone and diminish the asymmetry of EVAR.

Hess et al. reported that VOR gain increased with increasing frequency in normal subjects and in patients with bilateral vestibular loss [11]. In the current case, horizontal VOR was not induced by horizontal sinusoidal stimulation at 0.2 Hz, whereas VOR was induced by sinusoidal stimulation at 0.6 Hz; however, the eye movement patterns during horizontal nystagmus to the right side were superimposed on

the sinusoidal shape. This finding suggests the presence of directional preponderance to the right side. In addition, the eye movements during VOR induced by stimulation at 0.8 Hz showed a nearly normal shape without the presence of superimposed nystagmus. These findings suggest that an increase in the VOR gain induced by high-frequency sinusoidal stimulation may suppress the occurrence of nystagmus superimposed on the VOR recording.

In the current case, our patient complained of "jumbling of vertical direction" of objects in his visual field when in motion. ENG recording shows that vertical VOR was irregularly induced during stepping. In addition, numerous horizontal nystagmus beats were induced during EVAR, whereas vertical downbeat nystagmus was scarcely induced during OVAR. We have some possible explanations for these findings. One possibility is associated with surgical trauma. Since the vertical nystagmus during OVAR is considered to be indicative of saccular function, saccular function in our patient may have been adversely affected by the insertion of the CI into the scala vestibuli. The scala vestibuli is closer to the saccular macula than the ampulla of the lateral semicircular canal. Therefore, the scala vestibuli insertion of CI might be more invasive against the saccular macula than the ampulla crista in the lateral semicircular canal. The second possibility is the difference of stimulus intensity to the sensory cells in OVAR. Although the tilt angle of OVAR in our study was set at 15° for the patient's safety, the optimal tilt angle of OVAR is generally 30°. Therefore, the tilt angle (15°) in the OVAR may not be sufficient for evaluating the otolith function. Finally, remaining possibility may be due to anatomical position among the inner ear windows, sacculus and semicircular canal. Since EVAR or OVAR were not performed before pre-reinsertion of electrode, it is unclear whether severely reduced response during OVAR occurred before surgery. Since the inner ear windows are closer to the saccular macula than the ampulla of the lateral semicircular canal, the sacculus may be easily involved in inflammation in the middle ear. The remaining possibility is to be caused by vertical semicircular canal hypofunction. The otolith receptors such as saccule and utricle are known to contribute to the VOR when the head moves linearly. However, the vertical semicircular canal is considered to contribute to the VOR in response to the walking-induced vertical head rotations [12]. Recently, it has been reported that some patients with severely impaired semicircular canal and normal succular function complained of the vertical jumbling of object during walking. These phenomena suggest saccular VOR alone to be insufficient to maintain a stationary image of the surroundings during physiologic vertical head movement. We speculated that the vertical jumbling phenomenon in our patient may be elicited by reduced gain of the vertical semicircular canal-ocular reflex.

References

[1] Lin K, Marrinan MS, Waltzman SB, Roland Jr JT. Multichannel cochlear implantation in the scala vestibuli. Otol Neurotol 2006;27:634–8.

[2] Suga F, Lindsay JR. Labyrinthitis ossificans due to chronic otitis media. Ann Otol Rhinol Laryngol 1975;84:37–44.

[3] Kiefer J, Weber A, Pfennigdorff T, von Ilberg C. Scala vestibuli insertion in cochlear implantation: a valuable alternative for cases with obstructed scala tympani. ORL J Otorhinolaryngol Relat Spec 2000;62:251–6.

[4] Berrettini S, Forli F, Neri E, Segnini G, Franceschini SS. Scala vestibuli cochlear implantation in patients with partially ossified cochleas. J Laryngol Otol 2002;116:946–50.

[5] Steenerson RL, Gary LB, Wynens MS. Scala vestibuli cochlear implantation for labyrinthine ossification. Am J Otol 1990;11:360–3.

[6] deSouza C, Paparella MM, Schachern P, Yoon TH. Pathology of labyrinthine ossification. J Laryngol Otol 1991;105:621–4.

[7] Takahashi M, Igarashi M, Wright WK. Damped pendular rotation nystagmus after unilateral labyrinthectomy or unilateral lateral semicircular canal block in squirrel monkeys. J Otolaryngol 1976;6:157–65.

[8] Suzuki M, Saito Y, Ushio M, Yamasoba T, Hatta I, Nakamura M. Vestibulo-ocular reflex (VOR) preserved in bilateral severe vestibular malformations with internal auditory canal stenosis. Acta Otolaryngol (Stockh) 2007;127:1226–30.

[9] Goode CT, Maney DL, Rubel EW, Fuchs AF. Visual influences on the development and recovery of the vestibuloocular reflex in the chicken. J Neurophysiol 2001;85:1119–28.

[10] Fetter M, Zee DS, Proctor LR. Effect of lack of vision and of occipital lobectomy upon recovery from unilateral labyrinthectomy in rhesus monkey. J Neurophysiol 1988;59:394–407.

[11] Hess K, Baloh RW, Honrubia V, Yee RD. Rotational testing in patients with bilateral peripheral vestibular disease. Laryngoscope 1985;95:85–8.

[12] Brantberg K, Löfqvist L. Preserved vestibular evoked myogenic potentials (VEMP) in some patients with walking-induced oscillopsia due to bilateral vestibulopathy. J Vest Res 2007;17:33–8.

Neuroscience Letters 487 (2011) 12–16

Contents lists available at ScienceDirect

Neuroscience Letters

journal homepage: www.elsevier.com/locate/neulet

Hydrogen in drinking water attenuates noise-induced hearing loss in guinea pigs

Ying Lin [a], Akinori Kashio [b], Takashi Sakamoto [b], Keigo Suzukawa [b], Akinobu Kakigi [b], Tatsuya Yamasoba [b,*]

[a] Department of Otolaryngology and Head and Neck Surgery, Xijing Hospital, Xi'an, China
[b] Department of Otolaryngology and Head and Neck Surgery, University of Tokyo, Tokyo, Japan

ARTICLE INFO

Article history:
Received 14 July 2010
Received in revised form
17 September 2010
Accepted 23 September 2010

Keywords:
Temporary threshold shift
Oxidative stress
Cochlea
Hair cell

ABSTRACT

It has been shown that molecular hydrogen acts as a therapeutic and preventive antioxidant by selectively reducing the hydroxyl radical, the most cytotoxic of the reactive oxygen species. In the present study, we tested the hypothesis that acoustic damage in guinea pigs can be attenuated by the consumption of molecular hydrogen. Guinea pigs received normal water or hydrogen-rich water for 14 days before they were exposed to 115 dB SPL 4-kHz octave band noise for 3 h. Animals in each group underwent measurements for auditory brainstem response (ABR) or distortion-product otoacoustic emissions (DPOAEs) before the treatment (baseline) and immediately, 1, 3, 7, and 14 days after noise exposure. The ABR thresholds at 2 and 4 kHz were significantly better on post-noise days 1, 3, and 14 in hydrogen-treated animals when compared to the normal water-treated controls. Compared to the controls, the hydrogen-treated animals showed greater amplitude of DPOAE input/output growth functions during the recovery process, with statistical significance detected on post-noise days 3 and 7. These findings suggest that hydrogen can facilitate the recovery of hair cell function and attenuate noise-induced temporary hearing loss.

Exposure to loud noise may cause sensorineural hearing loss that can last for minutes, hours, days, or permanently, depending on the parameters of the acoustic overstimulation and the subject's susceptibility to noise exposure. Noise-induced temporary threshold shift (TTS) is a reversible elevation in hearing threshold that occurs after acoustic overstimulation. TTS can be an indicator of exposures that lead to permanent hearing loss after multiple, cumulative exposure events. Although the mechanisms underlying this phenomenon are not fully understood, it is widely accepted that direct mechanical damage and/or indirect metabolic alterations may be involved. Most notably, the generation of reactive oxygen species (ROS) [12], which may serve as triggers for necrosis or apoptosis, results in damage to the cochlear hair cells and the subsequent degeneration of auditory neurons. Thus, suitable antioxidants are desired to protect against oxidative damage in the inner ear. Pharmacological agents effective against TTS may have a potential clinical role in the prophylaxis of acute acoustic damage. However, most antioxidants have difficulty reaching the cochlear hair cells because of the blood–labyrinthine barrier.

Recent studies have revealed that molecular hydrogen mediates beneficial effects in different systems as an optimal antioxidant agent by selectively scavenging free hydroxyl radicals (•OH) [23,25]. Inhaled hydrogen gas can prevent or reduce pathological or biochemical changes in animal models of cerebral infarction [23], neonatal hypoxia ischemia [4], hepatic injury [9], intestinal ischemia injury [2], myocardial ischemia-reperfusion injury [11], cisplatin-induced nephrotoxicity [19], polymicrobial sepsis [26], and generalized inflammation [27]. Continuous consumption of hydrogen water can also protect against intestinal ischemia [29], neonatal hypoxia-ischemia [3], chronic allograft nephropathy [5] and acute pancreatitis [6]. It has also been shown to reduce atherosclerotic lesions in apolipoprotein E knock-out mice [24], inactivate oxidative stress in the brain of Parkinson disease rodents [7,8], and prevent stress-induced decline in learning and memory caused by chronic physical restraint [18]. Hydrogen-loaded eye drops can also protect the retina from ischemia-reperfusion injury [21]. A clinical study has shown that consuming hydrogen-rich water improves lipid and glucose metabolism in type 2 diabetes patients [14]. Furthermore, hydrogen-saturated culture medium can protect cochlear hair cells against antimycin A-induced oxidative stress *in vitro* [16].

Because of permeability and few side effects of molecular hydrogen, it is considered especially favorable as a component of inner-ear medicine. In the present study, therefore, we tested the

* Corresponding author at: Department of Otolaryngology and Head and Neck Surgery, Faculty of Medicine, University of Tokyo, Hongo 7-3-1, Bunkyo-ku, Tokyo 113-8655, Japan.
E-mail address: tyamasoba-tky@umin.ac.jp (T. Yamasoba).

0304-3940/$ – see front matter © 2010 Elsevier Ireland Ltd. All rights reserved.
doi:10.1016/j.neulet.2010.09.064

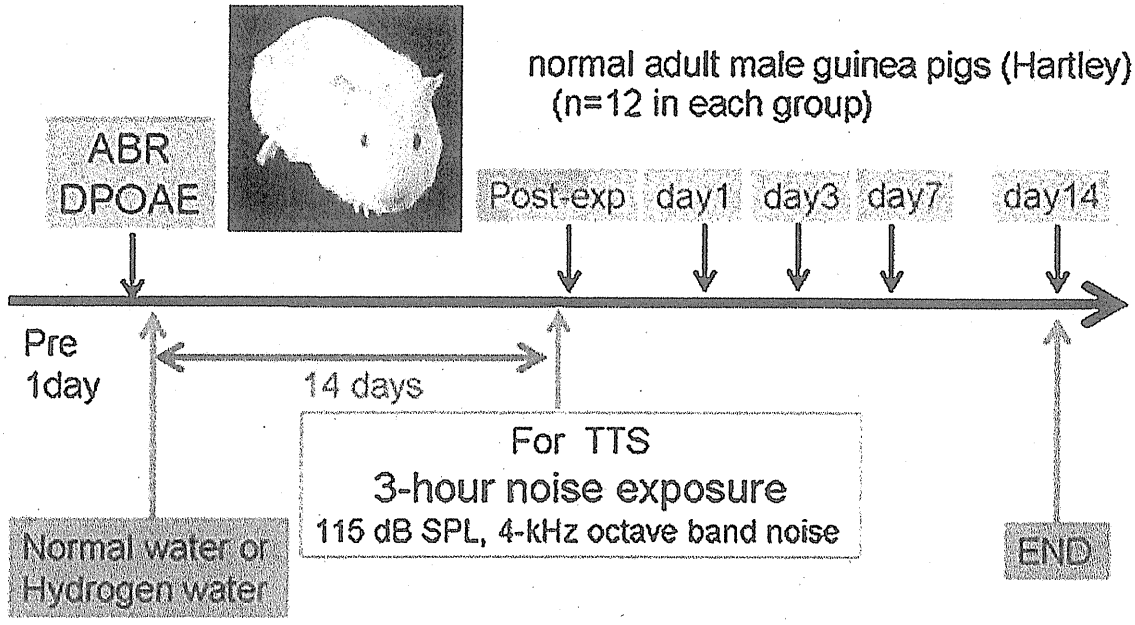

Fig. 1. Schedule of the experiment procedures.

hypothesis that continuous consumption of hydrogen water could attenuate noise-induced TTS in guinea pigs.

Thirty-four male Hartley guinea pigs weighing 250–300 g were used. Since sex differences have been associated with differing ability to detoxify ROS [13], only male guinea pigs were used. One day after arrival, their hearing was confirmed to be within the normal range (within one standard deviation of the normative laboratory baseline) with auditory brainstem response (ABR) or distortion product otoacoustic emissions (DPOAEs) measurements (Fig. 1). After the first baseline hearing tests, animals were randomly divided into normal water-treated and hydrogen water-treated experimental groups ($n = 17$ in each group). Treatment and control solutions were administered orally with unlimited access starting 14 days before noise exposure. Each day, supersaturated hydrogen water (Blue Mercury, Tokyo, Japan) was placed in a closed glass vessel, which minimizes the leakage of hydrogen from the water and maintains the concentration to be greater than 0.4 mM one day later [24]. Weight gains and amounts of water consumed were measured daily. This study was reviewed and approved by the Committee for Ethics in Animal Experiments of the University of Tokyo and carried out under Japanese law and the Guidelines for Animal Experiments of the University of Tokyo.

Fourteen days after starting, either normal or hydrogen water treatments, the animals were subjected to a 3-h noise exposure (115 dB SPL, 4 kHz octave band noise) generated within a single-walled, sound-deadened chamber as previously reported [28]. Two separately caged animals were tested simultaneously and allowed to move freely during exposure. The sound chamber was fitted with speakers driven by a noise generator and power amplifier. A 0.5-in. Bruel and Kjaer condenser microphone and a Fast Fourier Transform analyzer were used to measure and calibrate the sound level at various locations within the chamber to ensure stimulus uniformity within ±1 dB.

To assess the effect of hydrogen water on TTS, 24 animals ($n = 12$ in each group) were subjected to ABR measurements immediately and at 1, 3, 7, and 14 days after noise exposure. The method of ABR measurement has been described previously [15]. In brief, animals were anesthetized intramuscularly with a mixture of xylazine hydrochloride (10 mg/kg) and ketamine hydrochloride (40 mg/kg), and needle electrodes were placed subcutaneously at the vertex (active electrode), beneath the pinna of the measured ear (reference electrode), and beneath the opposite ear (ground). The stimulus duration was 15 ms; the presentation rate, 11/s; the rise/fall time, 1 ms; and the frequencies, 2, 4, 8, and 16 kHz. Responses of 1024 sweeps were averaged at each intensity level. The sound intensity was varied in 5 dB intervals at the intensities close to the threshold, which was defined as the lowest intensity level that produced a clear reproducible waveform peak 3 or 4. In general, amplitude at threshold was approximately 0.1 μV.

Ten animals ($n = 5$ in each group) underwent DPOAE measurement immediately and at 1, 3, 7, and 14 days after noise exposure with an acoustic probe using the DP2000 DPOAE measurement system version 3.0 (Starkey Laboratory, Eden Prairie, MN) as described previously [20]. DP-grams comprised 2f1–f2 DPOAE amplitudes as a function of f2. The stimulus paradigm used for DPOAE input/output (I/O) growth function is constructed as follows [10]: two primary tones with a frequency ratio, f2/f1, of 1.2 were presented, with f2 in one-sixth-octave steps from 1 to 16 kHz. At each frequency pair, primary levels of L2 were incremented in 5 dB steps from 40 to 70 dB SPL with an L1–L2 value of 10 dB. DPOAE was defined to be present when its level exceeded that of the noise floor by 3 dB.

The overall effects of the hydrogen treatment were examined using a two-way factorial analysis of variance with Bonferroni post-tests (SPSS software). p values of less than 0.05 were considered to be statistically significant. Values are expressed as the mean (standard deviation).

Weight gain and the amount of water consumed were not statistically different between the 2 groups (data not shown). Chronological alterations in the ABR threshold shifts at 2, 4, 8, and 16 kHz before and after noise exposure with the application of hydrogen-rich or normal water are shown in Fig. 2. ABR thresholds before noise exposure were essentially equivalent between the 2 groups. In normal water-treated controls, ABR thresholds were moderately increased by approximately 45 dB at all frequencies immediately after noise exposure. Subsequently the ABR thresholds showed gradual recovery, returning to pre-exposure baseline thresholds 14 days later, indicating that the noise exposure induced TTS. Hydrogen-treated animals showed similar but smaller ABR threshold shifts after noise exposure, as compared to the controls.

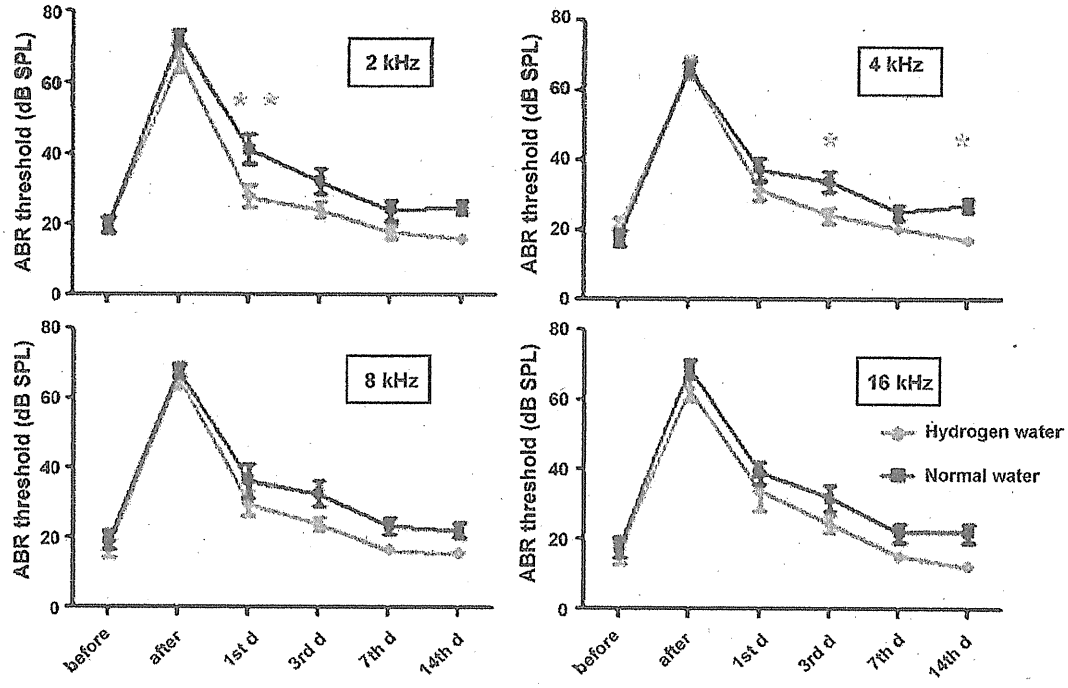

Fig. 2. Thresholds of auditory brainstem response (mean ± S.D.) measured before, immediately after noise exposure and post-noise 1st day, 3rd days, 7th days, 14th days in normal water-treated controls and hydrogen-treated animals ($n = 12$ in each group). There is a statistical significance at all frequencies (two-way ANOVA) and post-noise 1st day for 2 kHz, 3rd day and 14th day for 4 kHz with Bonferroni post-tests (**$p < 0.01$, *$p < 0.05$).

The overall effect of hydrogen significantly attenuated the TTS across the measurement period for all the tested frequencies ($p < 0.05$). Compared to the controls, the hydrogen-treated animals showed significantly smaller ABR thresholds at 2 kHz on day 1 day after noise exposure ($p < 0.01$) and at 4 kHz on day 3 and 14 after noise exposure ($p < 0.05$).

Fig. 3 shows the mean DPOAE input/output (I/O) growth functions at 16 kHz before and immediately, 1, 3, 7, and 14 days after noise exposure. There was no statistically significant difference between the 2 groups considering the amplitude of DPOAE I/O function. Both the groups showed a severe decrease in DPOAE amplitude immediately after noise exposure. Compared to the controls, the hydrogen-treated animals showed greater amplitudes during the recovery process. The overall effect of hydrogen water application was statistically significant 3 and 7 days after noise exposure ($p < 0.01$), although both groups exhibited almost normal I/O function 14 days after noise exposure.

The present study showed that hydrogen attenuated noise-induced TTS and accelerated the recovery of DPOAE. It is likely that hydrogen facilitates the recovery of hearing function because of its antioxidant property [1]. A previous *in vitro* study has also demonstrated the potential of hydrogen to protect both the inner hair cells and outer hair cells from oxidant damage induced by different concentrations of antimycin A [16]. Incubation with a hydrogen-saturated medium significantly reduced ROS generation and subsequent lipid peroxidation in the auditory epithelia, leading to increased survival of hair cells. Hydrogen selectively alleviates hydroxyl radicals (•OH) and peroxynitrite radical ($ONOO^-$)-induced cytotoxicity without affecting other ROS, such as superoxide ($O_2^{\bullet -}$), hydrogen peroxide (H_2O_2), or nitric oxide ($NO^\bullet$) [23]. Thus, it is unlikely that hydrogen disturbs metabolic oxidation–reduction reactions or disrupts ROS involved in cell signaling. This characteristic of hydrogen is advantageous in medical treatments because the use of hydrogen should not cause serious unwanted side effects.

In the current study, we did not examine the morphological changes in the cochlea because the abnormalities in ABR and DPOAE measurements were minimal 14 days after noise exposure. The physiological findings, however, suggest that the noise level used in the current study induced only subtle morphological changes such as bleb formation, but not severe degeneration such as apoptosis of the outer hair cells. No significant permanent morphological changes have been shown in the hair cells in previous studies using a similar protocol of noise exposure [22]. In contrast, it has been shown that in guinea pigs, the afferent dendrites beneath the inner hair cells become swollen immediately after exposure to similar noise causing TTS [28]. Kujawa and Liberman [17] have reported that acoustic overexposures causing moderate, but completely reversible threshold elevation leave cochlear sensory cells intact but cause acute loss of the afferent nerve terminals and delayed degeneration of the cochlear nerve in mice. Although the difference of ABR thresholds immediately after noise was small between hydrogen-treated animals and controls, therefore, it is considered intriguing to examine if hydrogen attenuates such acute and chronic changes of the neural elements.

The efficacy of any single antioxidant may be limited by several factors, including limited access to cellular compartments, action against only a few forms of ROS, interference with redox-based signaling, or a tendency to throw innate ROS protections out of balance [22]. Thus, despite its mild effect, molecular hydrogen is still an optimal choice. It reacts only with the strongest oxidants. Besides, it can penetrate biological membranes by gaseous rapid diffusion and target organelles like the mitochondria and nucleus, which makes it highly effective for reducing cytotoxic radicals. This unique feature of molecular hydrogen is especially favorable for drug delivery to the inner ear compared to other antioxidants, because the blood–labyrinthine barrier blocks many therapeutic compounds and does not allow them to reach cochlear hair cells.

The present study shows that hydrogen can promote hearing recovery from acoustic trauma-induced TTS and can attenuate TTS. This improvement likely reflects hydrogen's scavenging of detrimental ROS. Since hydrogen has already been used in humans clinically to treat decompression sickness in divers with few or no side effects, our findings reinforce the potential clinical utility of

Available online at www.sciencedirect.com
ScienceDirect
American Journal of OTOLARYNGOLOGY
ELSEVIER
American Journal of Otolaryngology–Head and Neck Medicine and Surgery 32 (2011) 215–220
www.elsevier.com/locate/amjoto

Cochlear changes in presbycusis with tinnitus☆

Kyoichi Terao, MD, PhD[a,b,d], Sebahattin Cureoglu, MD[a,c,*], Patricia A. Schachern, BS[a], Norimasa Morita, MD, PhD[a,b], Shigenobu Nomiya, MD, PhD[a,b], Armin F. Deroee, MD[a,b], Katsumi Doi, MD, PhD[d], Kazunori Mori, MD, PhD[d], Kiyotaka Murata, MD, PhD[d], Michael M. Paparella, MD[a,b,c]

[a]*Department of Otolaryngology, University of Minnesota, Minneapolis, MN, USA*
[b]*International Hearing Foundation, Minneapolis, MN, USA*
[c]*Paparella Ear Head and Neck Institute, Minneapolis, MN, USA*
[d]*Department of Otolaryngology, Kinki University School of Medicine, Osaka, Japan*

Received 3 October 2009

Abstract

Objectives: The pathophysiology of tinnitus is obscure and its treatment is therefore elusive. Significant progress in this field can only be achieved by determining the mechanisms of tinnitus generation, and thus, histopathologic findings of the cochlea in presbycusis with tinnitus become crucial. We revealed the histopathologic findings of the cochlea in subjects with presbycusis and tinnitus.

Material and methods: The subjects were divided into 2 groups, presbycusis with tinnitus (tinnitus) group and presbycusis without tinnitus (control) group, with each group comprising 8 temporal bones from 8 subjects. We quantitatively analyzed the number of spiral ganglion cells, loss of cochlear inner and outer hair cells, and areas of the stria vascularis and spiral ligament.

Results: There was a significantly greater loss of outer hair cells in the tinnitus group compared with the control group in the basal and upper middle turns. The stria vascularis was more atrophic in the tinnitus group compared with the control group in the basal turn.

Conclusions: Tinnitus is more common in patients with presbycusis who have more severe degeneration of outer hair cells and stria vascularis.

1. Introduction

Tinnitus is an auditory phantom sensation (ringing in the ears) experienced in absence of an external sound. According to a report of The American National Health, the prevalence of tinnitus was about 20% in Americans, which increased with age [1]. However, the pathophysiology of tinnitus remains obscure, and thus, its treatment is elusive.

Age-related hearing loss (presbycusis) is thought to result from age-related degeneration of the cochlea [2] and is a cause of peripheral tinnitus. There are many studies on presbycusis, but the histopathologic effect of presbycusis with tinnitus in human temporal bones has not been studied. Significant progress in this field will lead to better understanding of some of the possible tinnitus generation mechanisms. We therefore studied the correlation between tinnitus due to presbycusis and histopathologic changes in the cochlea.

2. Materials and methods

2.1. Subjects

The tinnitus group comprised 8 temporal bones from 8 subjects having presbycusis with tinnitus (6 males and 2 females; age range, 64–93 years; mean age ± SD, 79.4 ± 8.7 years; high-tone-loss pattern, 1 subject, and descending pattern, 7 subjects; mean bone-conductance thresholds ± SD, 40.4 ± 15.9 dB).

☆ Funding/support: This study was supported by the International Hearing Foundation, the Starkey Foundation, and the Society for Promotion of International Oto-Rhino-Laryngology.

* Corresponding author, Department of Otolaryngology, University of Minnesota, Room 210, Lions Research Building, 2001, 6th Street S.E., Minneapolis, MN 55455, USA. Tel.: +1 612 626 9883; fax: +1 612 626 9871.
E-mail address: cureo003@umn.edu (S. Cureoglu).

0196-0709/$ – see front matter © 2011 Elsevier Inc. All rights reserved.
doi:10.1016/j.amjoto.2010.02.001